

# The nonlinear non-parallel wave instability of boundary-layer flow induced by a horizontal heated surface in porous media

By D. A. S. REES<sup>1</sup> AND ANDREW P. BASSOM<sup>2</sup>

<sup>1</sup>School of Mechanical Engineering, University of Bath, Claverton Down, Bath, BA2 7AY, UK

<sup>2</sup>Department of Mathematics, University of Exeter, North Park Road, Exeter, Devon, EX4 4QE, UK

(Received 30 August 1991 and in revised form 11 December 1992)

The two-dimensional wave instability of convection induced by a semi-infinite heated surface embedded in a fluid-saturated porous medium is studied. Owing to the inadequacy of parallel-flow theories and the inaccuracy of the leading-order boundary-layer approximation at the point of incipient instability given by these theories, the problem has been re-examined using numerical simulations of the full time-dependent nonlinear equations of motion. Small-amplitude localized disturbances placed in the steady boundary layer are shown to propagate upstream much faster than they advect downstream. There seems to be a preferred wavelength for the evolving disturbance while it is in the linear regime, but the local growth rate depends on the distance downstream and there is a smooth, rather than an abrupt, spatial transition to convection.

The starting problem, where the temperature of the horizontal surface is instantaneously raised from the ambient, is found to give rise to a particularly violent fluid motion near the leading edge. A strong thermal plume is generated which is eventually advected downstream. The long-term evolution of the instability is computed. The flow does not settle down to a steady or a time-periodic state, and evidence is presented which suggests that it is inherently chaotic. The evolving flow field exhibits a wide range of dynamical behaviour including cell merging, the ejection of hot fluid from the boundary layer, and short periods of relatively intense fluid motion accompanied by boundary-layer thinning and short-wavelength waves.

---

## 1. Introduction

Convective flows in porous media are of interest in many varied situations such as in geothermal energy resource and oil reservoir modelling. The study of convection generated by a heated semi-infinite surface embedded in a saturated porous medium has attracted extensive treatment in recent years. Motivated by the need to model groundwater heating of an aquifer by an impermeable dike, Cheng & Minkowycz (1977) considered the flow induced by a vertical heated surface. By means of a boundary-layer theory they obtained a similarity solution for the case of an isothermal surface. Using the method of matched asymptotic expansions Daniels & Simpkins (1984) and Cheng & Hsu (1984) extended the boundary-layer theory to third order, thereby obtaining improved estimates of the Nusselt number. The analysis of convection induced by an upward-facing isothermal surface, which models heat transfer near a geothermal reservoir and which is of prime concern in this paper, has

followed a similar evolution. Cheng & Chang (1976) determined the leading-order boundary-layer flow, and this was extended later to third order by Chang & Cheng (1983). The corresponding analysis for arbitrarily inclined configurations (which also includes the effect of fluid inertia) is given in Riley & Rees (1985). Detailed reviews of much of this work are given in Cheng (1978) and Tien & Vafai (1989).

A recent study by Rees & Bassom (1991) has shown that some of the above-mentioned mathematical techniques are unnecessary for two particular configurations. This work examined a wedge-shaped region of saturated porous medium bounded by two semi-infinite surfaces, one heated isothermally, the other insulated. The two particular cases investigated were, firstly, a vertical surface with a wedge angle of  $\pi$  (i.e. both surfaces are vertical) and, secondly, a horizontal upward-facing surface with a wedge angle of  $\frac{3}{2}\pi$ . It was shown that, for both these configurations, the full nonlinear governing equations reduce to a set of ordinary differential equations upon introduction of appropriate transformations, and thus the basic steady flow in the whole flow domain is determined precisely. For other wedge angles the full steady two-dimensional equations of motion have to be solved.

Published work which addresses the stability of thermal boundary layers in *fluids* has considered primarily two possible disturbance types. The first is the development of Tollmien–Schlichting-like (i.e. two-dimensional) travelling waves within the boundary layer. The second concerns longitudinal spanwise-periodic vortex disturbances. In the context of thermal boundary layers in fluids, there have been several attempts to decide which disturbance type is the more important. For example, Iyer & Kelly (1974) investigated free convective flows induced by a heated inclined surface. They concluded that for inclinations close to the vertical the two-dimensional Tollmien–Schlichting disturbance is the more unstable mode whereas for inclinations of greater than  $4^\circ$  away from the vertical the vortex mode is the more unstable.

Stability analyses undertaken by Hsu, Cheng & Homsy (1978), Hsu & Cheng (1979) and Jang & Chang (1989) are concerned solely with vortex disturbances within boundary layers induced by heated surfaces embedded in porous media. Their concentration on vortex modes is motivated by experimental evidence which was referred to by Hsu *et al.* (1978) but not presented in their paper. After submission of the original manuscript of the present paper we undertook a wave-instability analysis of the horizontal configuration considered by Hsu *et al.* and found that, contrary to their cited experimental results, waves are more destabilizing than vortices. In particular, vortices are destabilizing beyond a non-dimensional distance of 33.47 from the leading edge, whilst the corresponding distance for waves is 28.90 (Rees & Bassom 1992). It must be pointed out, however, that these papers rely heavily on the validity of both the boundary-layer and the parallel-flow approximations. Concerning the boundary-layer approximation, it is well-known that the higher-order boundary-layer theory for the horizontal problem proceeds, at least initially, in powers of  $x^{\frac{1}{2}}$ , where  $x$ , the distance from the leading edge, is assumed to be large. Thus successive terms in the expansion differ in magnitude by a factor of roughly  $28.90^{\frac{3}{2}} \approx 3.07$  at the point of incipient instability for waves, and therefore the boundary-layer approximation is particularly inaccurate here.

For the present problem – the stability of horizontal thermal boundary-layer flow in a porous medium – it is not sufficient that further terms be included in the analyses of Hsu *et al.* or Rees & Bassom (1992), or even that the exact solution presented in Rees & Bassom (1991) be used as the basic flow, for the status of the parallel-flow approximation as a suitable means of determining the stability characteristics of spatially developing flows has been called into question in recent years. When

considering, for example, a spanwise-periodic (or vortex) perturbation to a basic boundary-layer flow, one formally obtains a partial differential system which has to be solved numerically in order to assess the stability characteristics of that flow. However, in order to simplify this task, it is frequently assumed in practice that the basic flow and/or the disturbance quantities take on some specified streamwise dependence; this is the essence of the parallel-flow approximation and it has the distinct advantage of reducing the linear stability equations to a set of ordinary differential equations whose solutions can be obtained relatively easily. In the context of the Görtler vortex instability of boundary-layer flows over curved surfaces, Hall (1982*a, b*) argued that an analysis of this type is flawed. He showed that the parallel-flow assumption is unjustifiable except in the limit of small vortex wavelengths. Moreover, in this case the Görtler instability may be described by an asymptotic structure which takes account of the boundary-layer growth in a rational manner and hence the parallel-flow assumption is rendered unnecessary in the only situation in which it has any relevance. Indeed, a later paper by Hall (1983) indicated that the governing parabolic partial differential system must be solved numerically, and showed two significant features of the non-parallel flow problem, namely, that the ideas of a unique stability curve and of a unique growth rate at a specified downstream location are inapplicable to the Görtler problem because the location at which a vortex begins to grow is dependent upon the position and shape of the imposed disturbance. Other work by the present authors (Bassom & Rees 1993) is aimed at investigating how non-parallel effects affect thermal boundary-layer instabilities in the form of longitudinal vortices in porous media.

The initial attempts at examining the stability of other fluid boundary layers to (two-dimensional) Tollmien–Schlichting waves were also based upon parallel-flow assumptions. The first rational investigation incorporating non-parallelism was presented by Smith (1979) who demonstrated, in contrast to the Görtler situation, that these non-parallel effects are relatively insignificant and, for many practical purposes, it is not essential that these conditions are accurately accounted for. It is worth remarking, however, that the non-parallel results derived by Smith (1979) are closer to the available experimental observations than are the corresponding parallelized ones. In more detail, Smith (1979) showed that non-parallelism manifests itself in the fourth terms of the expansions for neutrally stable Tollmien–Schlichting wavenumbers and frequencies when these quantities are expressed in terms of the (assumed asymptotically large) Reynolds number. Thus at such high Reynolds numbers the non-parallel results of Smith differ only slightly from their parallelized counterparts whereas for the Görtler non-parallelism has a leading-order influence and neglecting non-parallelism leads, in general, to completely erroneous conclusions. (A complete discussion of this point is elucidated in the review article by Hall 1990.) This work on fluid boundary layers suggests that at first sight the wave instability analysis for thermal boundary layers might after all be adequately described by a parallelized theory of the type alluded to above. However, there is a significant difference between the work of Smith (1979) and that discussed here in this paper; this contrast is associated with (i) the inaccuracy of the leading-order boundary-layer approximation used by previous analyses and (ii) the size of streamwise derivatives in the diffusion terms at the expected point of incipient instability.

In view of the above considerations it can be seen that, in order to assess the stability of thermal boundary layers in porous media, a careful study is required. It will be necessary eventually to examine the relative importance and stability characteristics of both wave and vortex instabilities, but here we begin the task by analysing two-

dimensional, or wave instabilities; this first step may be justified by the results of Rees & Bassom (1992), but in view of the size of the computational problem it is also the obvious initial step. The degree of inaccuracy of the leading-order boundary-layer approximation at the respective points of incipient instability given by Hsu *et al.* (1978) and Rees & Bassom (1992) is such that streamwise derivatives in the diffusion terms of the disturbance equations cannot be formally neglected, as is the case in the non-parallel Görtler vortex analyses of Hall (1982*a, b*, 1983). Therefore it was deemed necessary, at least initially, to abandon attempts at analytical progress, but to proceed entirely numerically. It is easier (relatively speaking, that is, though not easy in an absolute sense) to look at two-dimensional or wave instabilities, for although we expect that three-dimensionality will eventually ensue, in line with the behaviour of other boundary-layer flows, a fully three-dimensional time-dependent calculation is currently beyond our computer resources, and therefore two-dimensional wave calculations are presented here. However, should three-dimensional motions be found eventually to comprise the more important primary mode of instability, the computations we present remain valid for convection in an upright Hele–Shaw cell. Fortunately, fully nonlinear calculations and linear calculations are of equal difficulty, and therefore a fully nonlinear numerical code has been developed. To be specific, we consider the fate of the steady thermal boundary layer induced by an upward-facing horizontal surface embedded in a porous medium with a wedge angle of  $\frac{3}{2}\pi$ . We use the coordinate transformation presented in Rees & Bassom (1991) to transform the unsteady two-dimensional equations; the advantages that accrue are the following: the boundary layer has constant thickness in the new coordinate system, singular derivatives at the origin are taken into account exactly for this wedge angle, and the basic flow is easily computed, as mentioned previously.

The plan of the paper is as follows. In §2 we introduce the equations of motion, define the coordinate transformation used, and present the basic boundary-layer flow, while details of the numerical method used are given in §3. In §§4, 5 and 6 various facets of the numerical solutions are presented and discussed. We investigate three problems: (i) the evolution of small disturbances to the basic flow; (ii) the starting problem, where the non-dimensional temperature is everywhere zero, initially, and the temperature of the horizontal surface is suddenly raised; and (iii) the long-term convective dynamics. We discuss briefly our results in §7.

## 2. The basic flow, the local Rayleigh number and a preliminary discussion

The basic configuration we consider is as shown in figure 1. An infinite expanse of fluid-saturated porous medium is contained between two semi-infinite impermeable surfaces. A horizontal bounding surface ( $y = 0, x \geq 0$ ) is held at a non-dimensional temperature of 1 whilst the vertical bounding surface ( $x = 0, y \leq 0$ ) is insulated; the ambient temperature of the medium is zero. Assuming that Darcy's law and the Boussinesq approximation are both valid, the non-dimensional equations governing unsteady two-dimensional motion become

$$\psi_{xx} + \psi_{yy} = -\theta_x, \quad (1a)$$

$$\theta_t = \theta_{xx} + \theta_{yy} + \psi_x \theta_y - \psi_y \theta_x; \quad (1b)$$

see Riley & Rees (1985) for details of the non-dimensionalization. Since there is no natural lengthscale in the problem we have set the Darcy–Rayleigh number equal to 1; this, in effect, defines a dimensional lengthscale in terms of the material parameters of

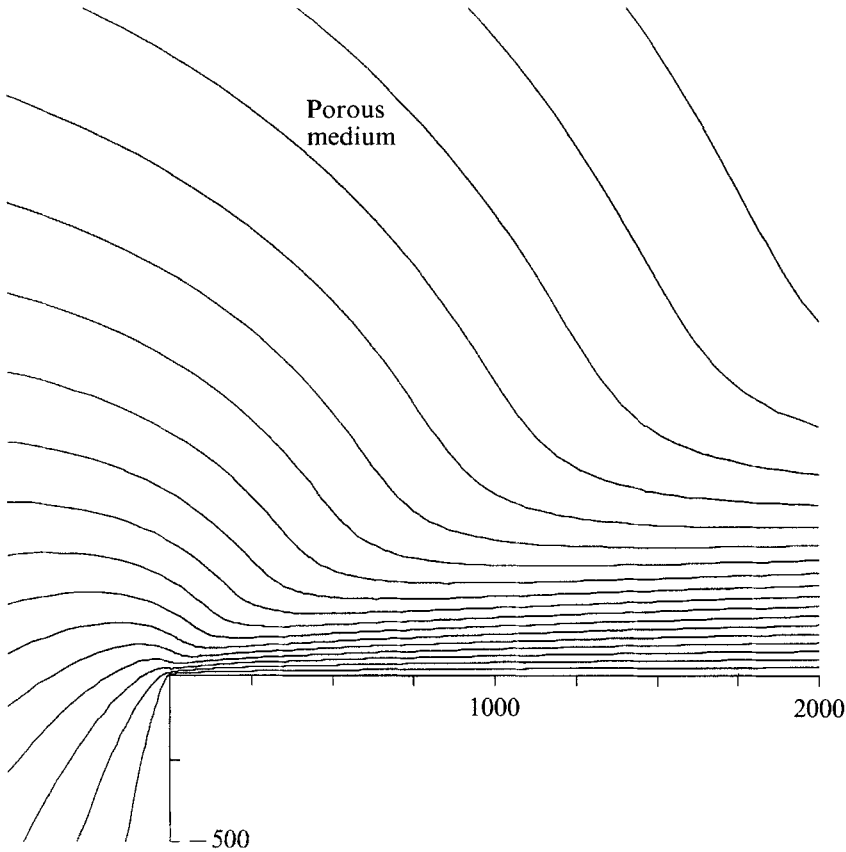


FIGURE 1. The configuration considered in this paper. Also shown are the streamlines of the steady boundary-layer solution.

the problem. In terms of polar coordinates defined by  $x = r \cos \phi$  and  $y = r \sin \phi$ , the boundary conditions are usually taken to be

$$\left. \begin{aligned} \psi = 0, \quad \theta = 1 \quad \text{on} \quad \phi = 0, \\ \psi = 0, \quad \frac{\partial \theta}{\partial \phi} = 0 \quad \text{on} \quad \phi = \frac{3}{2}\pi, \\ \theta \rightarrow 0, \quad \psi = o(r) \quad \text{as} \quad r \rightarrow \infty, \quad 0 < \phi < \frac{3}{2}\pi. \end{aligned} \right\} \quad (2)$$

In Rees & Bassom (1991) the change of coordinates,

$$\xi = 3r^{\frac{1}{3}} \cos\left(\frac{1}{3}\phi\right), \quad \eta = 3r^{\frac{1}{3}} \sin\left(\frac{1}{3}\phi\right), \quad (3a)$$

or, equivalently, 
$$x = \frac{\xi}{27}(\xi^2 - 3\eta^2), \quad y = \frac{\eta}{27}(3\xi^2 - \eta^2), \quad (3b)$$

were used to transform the steady form of (1 a, b). The unsteady equations become

$$\psi_{\xi\xi} + \psi_{\eta\eta} = \frac{1}{6}[2\xi\eta\theta_{\eta} + (\eta^2 - \xi^2)\theta_{\xi}], \quad (4a)$$

$$\theta_t = \frac{81}{(\xi^2 + \eta^2)^2}[\theta_{\xi\xi} + \theta_{\eta\eta} + \psi_{\xi}\theta_{\eta} - \psi_{\eta}\theta_{\xi}], \quad (4b)$$

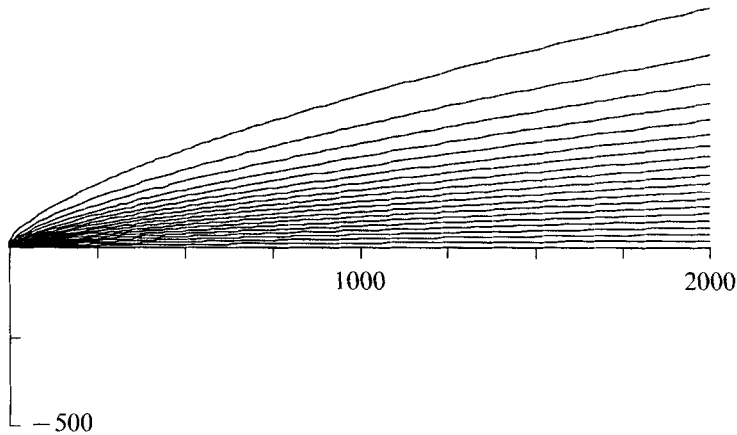


FIGURE 2. Isotherms of the basic boundary-layer solution plotted with an interval of 0.05 between adjacent contours.

and the basic, steady, boundary-layer flow can be seen to be given by

$$\psi = \frac{1}{3}\xi f(\eta), \quad \theta = g(\eta), \quad (5)$$

where  $f(\eta)$  and  $g(\eta)$  satisfy

$$f'' - \frac{2}{3}\eta g' = 0, \quad g'' + \frac{1}{3}f g' = 0, \quad (6a, b)$$

subject to the boundary conditions

$$f(0) = 0, \quad g(0) = 1 \quad \text{and} \quad f', g \rightarrow 0 \quad \text{as} \quad \eta \rightarrow \infty. \quad (6c)$$

Equations and boundary conditions (6a–c) were first obtained and solved numerically by Cheng & Chang (1976) in their study of the leading-order boundary-layer flow far downstream from the leading edge. As the expressions for  $\psi$  and  $\theta$  given in (5) satisfy the full, steady form of (4a, b), and not the boundary-layer approximation to (1), Cheng & Chang's similarity solution can be used to determine the whole flow field, given the present definition of  $\xi$  and  $\eta$ . However, this conclusion only applies when the wedge angle is equal to  $\frac{3}{2}\pi$ ; corresponding solutions for other wedge angles must be obtained numerically or approximated in the usual way using boundary-layer theory. In this paper we confine our attention to the  $\frac{3}{2}\pi$  case, as shown in figure 1, since solutions are easier to compute for this particular case.

Plots of the streamlines and isotherms corresponding to the steady basic flow are shown in figures 1 and 2 and the development of the boundary layer as  $x$ , the distance along the heated surface, increases can be seen clearly. It is important to reiterate a point made in Rees & Bassom (1991) that there is one aspect of the mathematical model which is not evident in these figures, namely, that the radial derivatives of both  $\psi$  and  $\theta$  become singular as  $r \rightarrow 0$ . This follows because

$$\psi = \frac{3}{2}r^{\frac{3}{2}} \sin\left(\frac{3}{2}\phi\right) f'(0) + O(r), \quad (7a)$$

$$\theta = 1 + 3r^{\frac{1}{2}} \sin\left(\frac{3}{2}\phi\right) g'(0) + O(r^{\frac{3}{2}}), \quad (7b)$$

for small  $r$ , where  $f'(0) \approx 1.0557$  and  $g'(0) \approx -0.4302$ . In terms of  $\xi$  and  $\eta$ , though, all derivatives are finite since both  $\psi$  and  $\theta$  can be expanded in a Taylor series in  $\xi$  and  $\eta$  about the origin. In fact it may be shown easily that, for small  $\xi$  and  $\eta$ ,  $\psi \sim \frac{1}{6}\xi\eta f'(0)$  and  $\theta \sim 1 + \eta g'(0)$ . Thus the  $(\xi, \eta)$ -coordinate system is the natural one to use for this problem.

It proves useful to define a local Rayleigh number based on the boundary-layer thickness so that the numerical results presented later can be interpreted in the light of known work on the porous-medium analogue of the Bénard problem (Lapwood 1948). Clearly such a local Rayleigh number will be precisely equal to the local boundary-layer thickness which we shall take to be where  $\theta = 0.05$ , that is, at  $\eta = 4.13$ . Therefore, at any given station,  $x$ , downstream of the leading edge, the local Rayleigh number,  $Ra(x)$ , is defined here to be that value of  $y$  for which  $\eta = 4.13$ . A plot of  $Ra(x)$  is shown in figure 2 as the  $\theta = 0.05$  isotherm, and it can be seen that, not surprisingly,  $Ra(x)$  is an increasing function of  $x$ . In the porous-Bénard (or Lapwood) problem convection ensues when the Rayleigh number is greater than  $4\pi^2$  and the paper by Prats (1967) assures us that a uniform horizontal flow does not affect the convective dynamics but results in the whole pattern being translated uniformly downstream. In view of this, one should not expect convective instability to arise for the present problem when  $Ra(x) < 4\pi^2$  (or, when  $x < 14.38$ ), and one would expect convection in the form of travelling cells otherwise. The transition to convection should then be smooth rather than abrupt (see Walton 1985 who considers convection in a fluid layer of slowly increasing depth in the presence of a weak shear flow). If this *a priori* reasoning provides a true qualitative description of the instability then the resulting motion should be periodic in time once the initial transients have decayed. However, when  $Ra(x) > 225$  (or, when  $x > 366.9$ ), Lapwood convection itself becomes periodic (Riley & Winters 1991), suggesting various possibilities for the present problem: some form of frequency locking between the unsteady Lapwood-type motion and the travelling wave motion; a quasi-periodic flow where the two types of unsteady motion are essentially uncoupled; a chaotic motion. The resulting unsteady motion should also affect the flow at lower values of  $Ra(x)$ . However, we shall see later that this *a priori* account of the dynamics of the flow is almost entirely incorrect. In pursuing the analogy between the Lapwood problem and the present problem there are two essential differences which we suspect are vitally important. The first is that the boundary layer is confined to the region near the boundary by means of a flow into the boundary layer, rather than by an impermeable boundary as in the Lapwood problem. If this inflow is weakened locally the thermal boundary layer should expand locally and form an embryonic plume. The second is that the convective cells in the present problem must expand horizontally as they travel downstream for the analogy to hold. This turns out not to be the case, for once a cell has entered the nonlinear regime it seems to resist any change in wavelength. Later we shall see that the evolving nonlinear state exhibits many unusual characteristics and does not settle down to a periodic motion.

### 3. The numerical method

The numerical scheme chosen to solve equations (4) is an implicit scheme, and we discuss this in detail below. Though explicit methods are attractive, because of their relative ease of programming, it is entirely impractical to use them for the problem we are considering here. This statement can be justified as follows. For a typical two-dimensional evolution problem, such as that of unsteady heat conduction governed by the equation

$$T_t = T_{xx} + T_{yy}, \quad (8)$$

explicit methods have a restriction on the size of the time step which is dictated by stability requirements. Typically the time step must be smaller than a multiple of the square of the spatial step. Here we are solving (4), which is a nonlinear system unlike

(8), but much greater significance must be attached to the fact that the right-hand side of (4b) is multiplied by the spatially varying factor  $81/(\xi^2 + \eta^2)^2$ . This factor may be regarded as a spatially varying thermal diffusivity in the new coordinate system. It is reasonable, therefore, to expect that there will be a very large spatial variation in the natural timescales in the flow. Now when both  $\xi$  and  $\eta$  are small, as is the case near the leading edge, the factor is large, and the temperature field evolves quickly. Far from the leading edge, where one would expect all the interesting dynamics to occur, the factor is small and the temperature field is relatively static. This can be illustrated by considering a typical case examined later for which we take the spatial steps  $\delta\xi$  and  $\delta\eta$  both equal to 0.25,  $\xi_{\max} = 30$  and  $\eta_{\max} = 15$ . Using these values the ratio of the local ‘thermal diffusivities’ near to, and far from, the leading edge is equal to  $8.1 \times 10^7$ , which can be interpreted as the ratio between the fastest and slowest timescales in the flow. Crudely speaking, the stability of an explicit method is based on the fastest timescale in a problem. For the present problem this occurs near the leading edge where the ‘local diffusivity’ is proportional to the inverse fourth power of the spatial step and therefore the time step for an explicit method must be proportional to the sixth power of the spatial step. In view of this stability requirement, which is extremely restrictive, and the fact that a Poisson solver has to be applied at each time step, it was decided that an implicit scheme must be used. It is also worth noting that the DuFort–Fraenkel method (which is technically implicit and unconditionally stable when solving linear evolution equations on rectangular domains) becomes conditionally stable when applied to nonlinear problems similar to those considered here; see Rees & Riley (1986) for one example of this. Thus the DuFort–Fraenkel method cannot be used here.

At first it was thought that the safest way of obtaining an unconditionally stable method was to use a first-order method based on a backward difference in time. Denoting the value of  $t$  at the  $n$ th time step as  $t_n$ , equation (4a) was discretized at  $t = t_{n+1}$  using the usual five-point finite difference star for the Laplacian and central differences for the first-order derivatives. The left-hand side of (4b) was approximated by  $(\theta_{ij}^{n+1} - \theta_{ij}^n)/\delta t$  and the right-hand side by the five-point star for the Laplacian and the Arakawa (1986) scheme for the advection terms – both were applied at  $t = t_{n+1}$ . This procedure was found to be unconditionally stable, but a second-order method similar to this, where all the terms are discretized at  $t = \frac{1}{2}(t_n + t_{n+1})$ , was also found, numerically, to be stable. For this second-order scheme the discretization of (4a) is the same as for the first-order method, but the time-independent terms of (4b) are approximated by taking the mean of their respective spatial discretizations at  $t = t_n$  and  $t = t_{n+1}$ , in the spirit of the Keller-box method (see Keller & Cebeci 1971). Both these methods were used extensively with very little numerical difference between their results.

Quite clearly the computation of  $\psi$  and  $\theta$  at each time step using one of these implicit methods is a substantial task, especially when the number of grid points is large – the largest number we report here is, in fact,  $97 \times 49$ . At each time step the finite difference equations were solved using pointwise Gauss–Seidel as the smoothing operator, and iterative convergence was accelerated using a standard Full Approximation Scheme multigrid algorithm with V-cycling over four grids. No advantage was found in either over- or under-relaxing the iteration scheme. Further details of the implementation of such a multigrid algorithm may be found in Brandt (1984). Typically the algorithm converged after 20 to 40 V-cycles, but sometimes, especially when following the initial stages of the evolution of small disturbances, it took as few as 10 V-cycles. In order to maximize the use of computer resources a rough form of time step control was used:

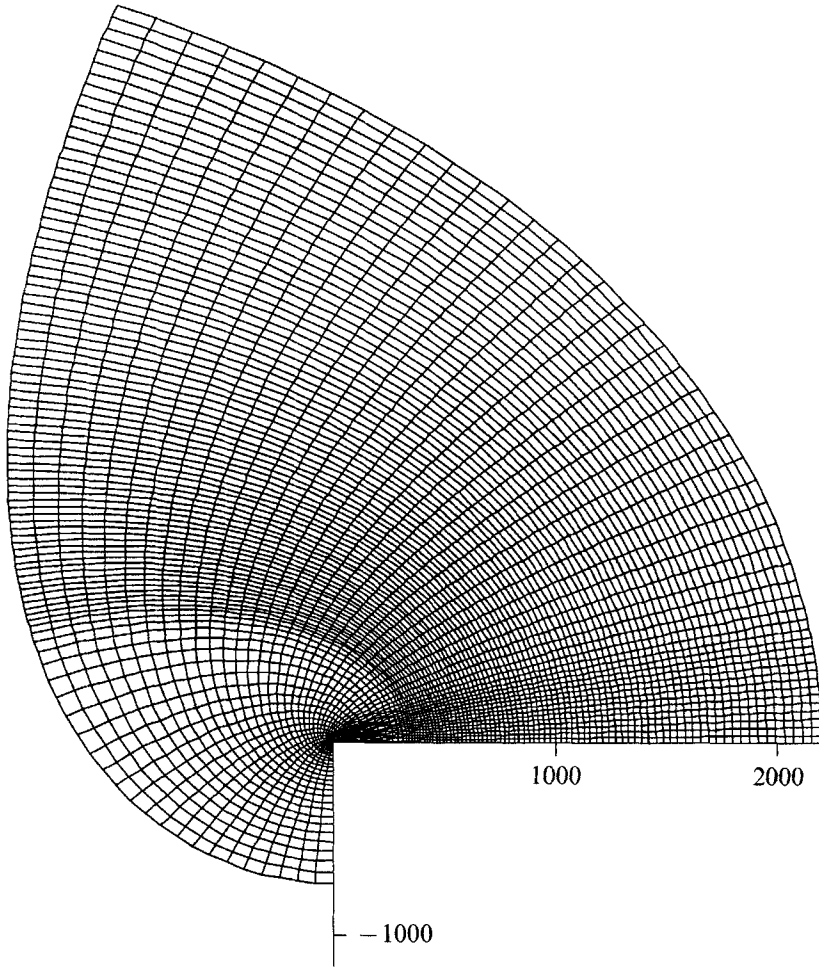


FIGURE 3. The computational grid showing the effects of the coordinate stretching transformations defined in the Appendix.

(i) if the maximum pointwise change in  $\theta$  between time steps is too large (small) then the time step is reduced (increased) on the next time step; (ii) the time step should not exceed 100 (this may seem very large, but the effective local timescale is dependent on the local ‘thermal diffusivity’) – this ensures that there is very little difference between the first- and second-order methods and thereby satisfies the need for temporally accurate solutions; (iii) the time step cannot increase by a factor of more than 2. The initial development of the code and preliminary computations were undertaken on a Sun SPARCstation SLC, but the work described in §6 was computed on an Intel i860 processor, which was roughly three times faster.

After the development of the code it was found that little dynamical activity takes place near the leading edge where  $\xi$  is less than roughly 15, and therefore an option to stretch the grid near  $\xi = 0$  was included in the code in order to optimize the use of computational resources. Similarly the grid lying in the range  $\eta > 3$  was stretched. The final stretched grid used is displayed in figure 3.

The question of spatial accuracy is of particular importance. Clearly, the use of the largest possible number of grid points commensurate with an adequate spatial resolution and a sufficiently short run-time precludes a further halving of the spatial

step. The use of a smaller domain was found to restrict the flow-field too much – a smaller value of  $\eta_{\max}$  was found not to allow the easy passage of buoyant hot spots out of the computational domain, and a smaller value of  $\xi_{\max}$  imposes temporal periodicity on the long-term dynamics. An examination of the spatial resolution of individual frames in figure 10 shows that the present computations are adequate. However, a doubling of the spatial step would yield an unacceptably coarse grid. Ideally we would like to undertake further computations with a finer grid over a larger domain but we are unable to do so at this point.

Finally it is necessary to comment on the boundary conditions applied to the problem. Obviously we have taken  $\psi = 0$ ,  $\theta = 1$  on  $\eta = 0$ , and  $\psi = 0$ ,  $\theta_\xi = 0$  on  $\xi = 0$ , but the choice of boundary conditions to apply to the other boundaries requires some discussion. We note that such a choice for general external flow problems is currently the subject of some considerable debate; see Kleiser & Zhang (1991) and references cited therein. Our experience with the code suggested that there was little need to transform the  $\eta$ -coordinate in such a way that its unbounded domain is mapped to a finite one. The value  $\eta_{\max} = 15$  was usually sufficiently large. At  $\eta = \eta_{\max}$  the condition  $\theta = 0$  was applied, to model the ambient temperature of the medium, and also  $\psi_\eta = 0$ , since the basic flow satisfies this condition. With regard to this latter condition,  $\eta_{\max}$  was always chosen sufficiently large that the  $\psi = \text{constant}$  contours are parallel to the lines  $\xi = \text{constant}$ , not just at the boundary but also for some distance into the domain. A more difficult problem was the choice of conditions at  $\xi = \xi_{\max}$ . It was eventually decided to set  $\psi_{\xi\xi} = 0$  and  $\theta_\xi = 0$  there; one reason for this is that these conditions seemed to be the most passive choice with regard to the effect on the resulting flow patterns and isotherms. Another, perhaps more important, reason is that the  $\psi_{\xi\xi} = 0$  condition gives the streamline field the greatest amount of freedom possible. We found that if the same reasoning were applied to the temperature condition then setting  $\theta_{\xi\xi} = 0$  gave very satisfactory results whenever there was outflow at the boundary. When inflow occurred, it was subsequently amplified and the whole flow field changed from being a horizontal boundary layer into one generating a persistent strong thermal plume. It cannot be emphasized too strongly that the boundary conditions we have chosen are imperfect since they cannot reflect accurately the detailed flow in  $\xi > \xi_{\max}$  and/or  $\eta > \eta_{\max}$ , but the process of choosing has the nature of a damage limitation exercise; we believe that the ‘damage’ is not too significant, except where indicated in the text, but since the only means available to us to validate the choice lies in performing subsequent computations with increasingly larger domains, one can never be fully satisfied with the numerical results obtained, at least for long-time simulations.

#### 4. The linear evolution of small disturbances

In this section we describe the initial evolution of small disturbances to the basic boundary-layer flow. The numerical procedure followed was fairly straightforward. Computations were performed on a  $121 \times 33$  grid which was uniform in the  $\xi$ -direction and non-uniform in the  $\eta$ -direction. We took  $\xi_{\max} = 30$  and  $\eta_{\max} = 15$ . It is necessary to note that in terms of the stretched  $\eta$ -coordinate,  $\bar{\eta}$  (see the Appendix for its definition),  $\bar{\eta}_{\max} = 8$ , and therefore we use a square grid with mesh length 0.25. Indeed, we use this mesh length in all the computations reported in this paper. The easiest way to obtain the basic profile is to solve the unsteady problem with  $\xi_{\max} = 4$ , which lies well within the range of stable local Rayleigh numbers. The resulting steady temperature profile, which is independent of  $\xi$ , was then extended by duplication to

$\xi_{\max} = 30$ . One further time step of length  $\delta t = 0.1$  was computed using the first-order method to compute the streamfunction (note that the first-order method does not rely on the previous values of the streamfunction and therefore this step does not change the temperature field). A small perturbation of the form

$$\theta_{\text{pert}} = \frac{B}{4} \left[ 1 - \cos \left( 2\pi \frac{\xi - a}{b - c} \right) \right] \left[ 1 - \cos \left( 2\pi \frac{\eta}{c} \right) \right], \quad a < \xi < b, \quad 0 < \eta < c, \quad (9)$$

with  $\theta_{\text{pert}} = 0$  elsewhere, was then introduced into the temperature field and its evolution followed. The results we present are shown in figures 4(a) and 4(b), and represent the evolution of the perturbation temperature field.

In these figures the perturbation expands slightly in the  $y$ -direction and spreads its influence both upstream and downstream. Somewhat surprisingly the upstream perturbation field is initially stronger than that downstream of the original perturbation, although this is true only in the initial stages of linear growth. The upstream propagation of the perturbation field is also considerably faster than the speed of advection of the evolving pattern downstream. This could, of course, be explained in terms of discrete modes by appealing to the ‘fact’ that the initial disturbance is composed of a set of discrete modes all of which decay, except perhaps one, thus giving the impression of a relatively fast upstream propagation. Whilst we believe there is a sizeable element of truth in this explanation it nevertheless begs the question of what is meant by a mode. Such a question can be answered easily by considering the Bénard and Lapwood problems for which the linear mode is periodic in space and has an amplitude and growth rate which are independent of the spatial coordinates. Even in configurations with spatial non-uniformities, such as in Walton’s (1982) work on convection in a layer with gradually increasing depth, a spatially periodic mode can be defined, and both the amplitude and linear growth rate are weakly spatially dependent. In the present problem, however, the depth of the boundary layer exhibits an  $O(1)$  variation, the planform is non-periodic and the growth rate is strongly dependent on spatial location. Therefore any use of the concept of ‘mode’ must be undertaken with a lack of mathematical precision at present. Returning to the fact that there is an upstream propagation of the disturbance, it is clear that such behaviour can only occur in a mathematical model which is elliptic in space. Thus a two-dimensional instability analysis using a parabolic method would necessarily give incorrect results since there is then no mechanism for upstream propagation.

Of some considerable interest is the observation that the evolving disturbances shown in figure 4 tend towards a state with roughly the same wavelength even though the initial disturbances have quite different streamwise widths. This observation is reminiscent of a result of Eagles (1980) who studied the effect of a  $\text{sech}^2$  lower boundary profile on the onset of Bénard convection. He showed that the presence of a spatially non-uniform, slowly varying boundary profile causes the subsequent convective motion to have a precise wavelength, unlike the corresponding case of uniform boundaries. In figure 4(a) the tall thin perturbation widens, whereas, in figure 4(b), the fat cell reduces its streamwise width. Indeed, in figure 4(b), the  $\theta_{\text{pert}} = 0$  contour initially travels upstream before beginning its slow advection downstream.

Space does not permit the inclusion of further graphical results of the evolution of disturbances but a few words should suffice. Perturbations similar to those already considered, but which are placed much nearer the leading edge, tend to decay initially but still advect downstream as before. When a perturbation is placed near the outflow boundary,  $\xi = \xi_{\max}$ , it has the advantage of having its maximum amplitude at the point

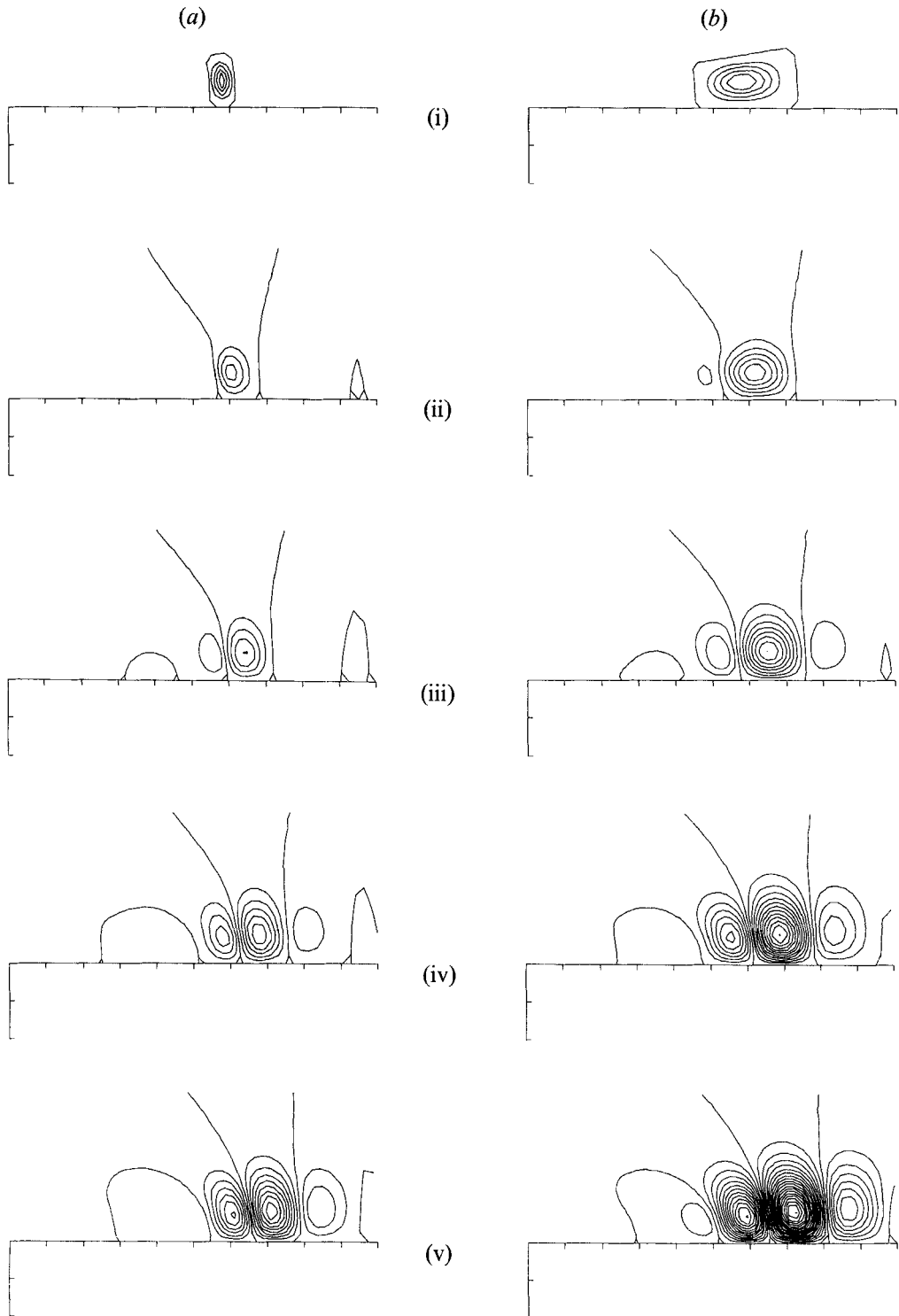


FIGURE 4. Perturbation isotherm contours for the disturbance defined by equation (9) with (a)  $a = 24.5$ ,  $b = 25.5$ ,  $c = 2$ ; and (b)  $a = 23$ ,  $b = 27$ ,  $c = 2$ . Contours are at an interval of 0.0002, and tick marks are at intervals of 100. (i)  $t = 0$ ; (ii)  $t = 327$ ; (iii)  $t = 627$ ; (iv)  $t = 927$ ; (v)  $t = 1227$ .

of largest linear growth rate within the computational domain. Subsequent development appears to be concentrated near the outflow boundary, but its presence is transmitted upstream where it grows relatively slowly. Should the perturbation be placed away from the horizontal surface but still within the boundary layer it retains all the evolutionary characteristics exhibited in figure 4 but also quickly spreads downwards towards the boundary. Finally, if the perturbation is placed well outside the boundary layer it advects downstream and heat diffuses from it. The streamline field is distorted slightly by its presence, however, and this is felt by the boundary layer. The isotherms subsequently become increasingly more distorted and the instability grows in strength.

It is necessary at this point to comment on how our linear results compare with previous work. In figure 4 it may be seen that very little activity takes place in the region  $x < 230$  (or  $\xi < 18$ ). In their paper, Hsu *et al.* (1978) predicted vortex instability near  $x = 33$  (or  $\xi \approx 10$ ) and we (Rees & Bassom 1992) predicted wave instability near  $x = 28$  (or  $\xi \approx 9$ ), stations which are much closer to the leading edge than that given by the present results. Without further information this appears to suggest that linearized results based on the parallel-flow approximation are quantitatively at variance with our simulations of the full equations. However, at the moment we suspect that the inclusion of streamwise derivatives in a linear theory is likely to give quite different qualitative, rather than quantitative, information from that obtained by neglecting such derivatives. To illustrate this point consider the equation

$$A_t = (R - X^2)A + A_{XX} - 2A^3,$$

which represents weakly nonlinear Bénard convection near a hot spot (Walton 1985). Standard linear theory for this equation assumes a zero growth rate and critical values of  $R$  are determined by solving

$$(R - X^2)A + A_{XX} = 0$$

with  $A$  not identically zero. The present problem is akin to setting a value of  $R$  and retaining the time derivative. Suppose that an initial condition  $A = \hat{A}(X)$  is given, with  $\hat{A}(X)$  being the eigenmode corresponding to an eigenvalue  $\hat{R}$  of the above linearized equation, then the solution of

$$A_t = (R - X^2)A + A_{XX}$$

is precisely

$$A = e^{(R-\hat{R})t} \hat{A}(X).$$

Hence when  $R > \hat{R}$  the solution grows everywhere. At present we think that a similar phenomenon occurs here because streamwise derivatives are retained in the diffusion terms. Our computed results in this section were initiated with a disturbance of amplitude  $B = 10^{-6}$  (see (9)) and the disturbance enters the nonlinear regime before propagating far upstream. Computations using our nonlinear code become difficult with smaller initial amplitudes. However, preliminary results for a linearized vortex analysis using a modified version of the code indicate that disturbances do in fact propagate towards the leading edge and thereafter continue to grow even at the leading edge. In these latter calculations it is not unusual for the disturbance to grow in amplitude by a factor of  $10^{20}$ . We intend to report on these matters in much more detail elsewhere, but we conclude for the moment that the retention of streamwise derivatives in the diffusion terms causes unstable modes to grow in the whole computational domain. In effect, this means that the critical distance beyond which disturbances grow is zero, for both waves and vortices. It would seem therefore that a proper comparison

of the relative importance of waves and vortices can only be ascertained by means of a fully nonlinear theory whenever streamwise derivatives are retained in the diffusion terms.

## 5. The starting problem

In this section we look at the flow and temperature field induced by suddenly raising the temperature of the horizontal surface to unity when the configuration is initially at the uniform temperature zero. The solution of a similar problem for a horizontal surface of infinite extent can be determined easily, where the temperature can be expressed in terms of the error function of the variable  $(y/t^{1/2})$ , and there is no flow. Far from the corner of the present system one would expect this solution to be valid, at least for sufficiently small times, but the main interest here is to determine numerically the effect of the corner on the development of the temperature field.

Solutions were obtained on precisely the same grid as was described in the preceding section. The reason for the choice of a constant step length in the  $\xi$ -direction was to allow for the intense initial activity which takes place near the corner. Again we have used the first-order method because, in practice, we found that at the corner the method has similar stability characteristics to the Backward Euler scheme for ordinary differential equations in as much that transients decay quickly to zero. The second-order method was found to be similar to the Modified Euler method; transients oscillate about a mean value with little or no decay. This was regarded as being unsuitable for this particular computation where the flow near the corner is of special interest. Given the analytical solution of the infinite surface problem it is clear that a very-small-time numerical solution on a stationary grid will be inaccurate due to an inadequate spatial resolution. Indeed this lack of resolution was found to give rise to negative (albeit of very small magnitude) temperatures over the first few time steps. However this was not thought to be too serious, for as the evolution proceeded the temperature field became positive everywhere.

In figure 5(*a-c*) we show the instantaneous streamlines and isotherms soon after the jump in the boundary temperature. Figure 5(*a*) corresponds to the initial, linear regime where the temperature field is dominated by diffusion. The fluid motion acts in immediate response to the developing temperature field. It should be noted that the irregular kinks in the isotherms away from the corner are merely an artifact of the  $(\xi, \eta)$ -coordinate system used in the computation. The fluid motion corresponding to figure 5(*a*) is beginning to deform the isotherms upwards; this is seen more clearly in figure 5(*b*), where the beginnings of a thermal plume is quite evident. A small region of clockwise recirculation is then established downstream of the plume serving to deform the isotherms further and enhancing the plume; see figure 5(*c*).

We reproduce figure 5(*c*) in figure 6(*a*) with a much smaller scale. Near  $\xi_{\max}$  in figure 6(*a*) a relatively weak recirculating region has been induced. Ideally this should not be present since the evolving temperature field far from the corner should be independent of  $x$  and would then satisfy the boundary condition  $\theta_x = 0$ . The boundary condition applied at  $\xi_{\max}$  is, however,  $\theta_\xi = 0$ , and the inevitable small perturbation there begins to grow. Its further growth can be seen in figure 6(*b, c*), but of more importance is the activity near the corner where the plume is developing further and continuing to rise. In figure 7(*a, b*) we reduce the scale still further and these figures show that the plume is now well outside the developing boundary layer. It would seem that the plume now has only a small effect on the evolution of the well-established boundary layer, though the fluid motion induced by the boundary layer will still strongly affect the development

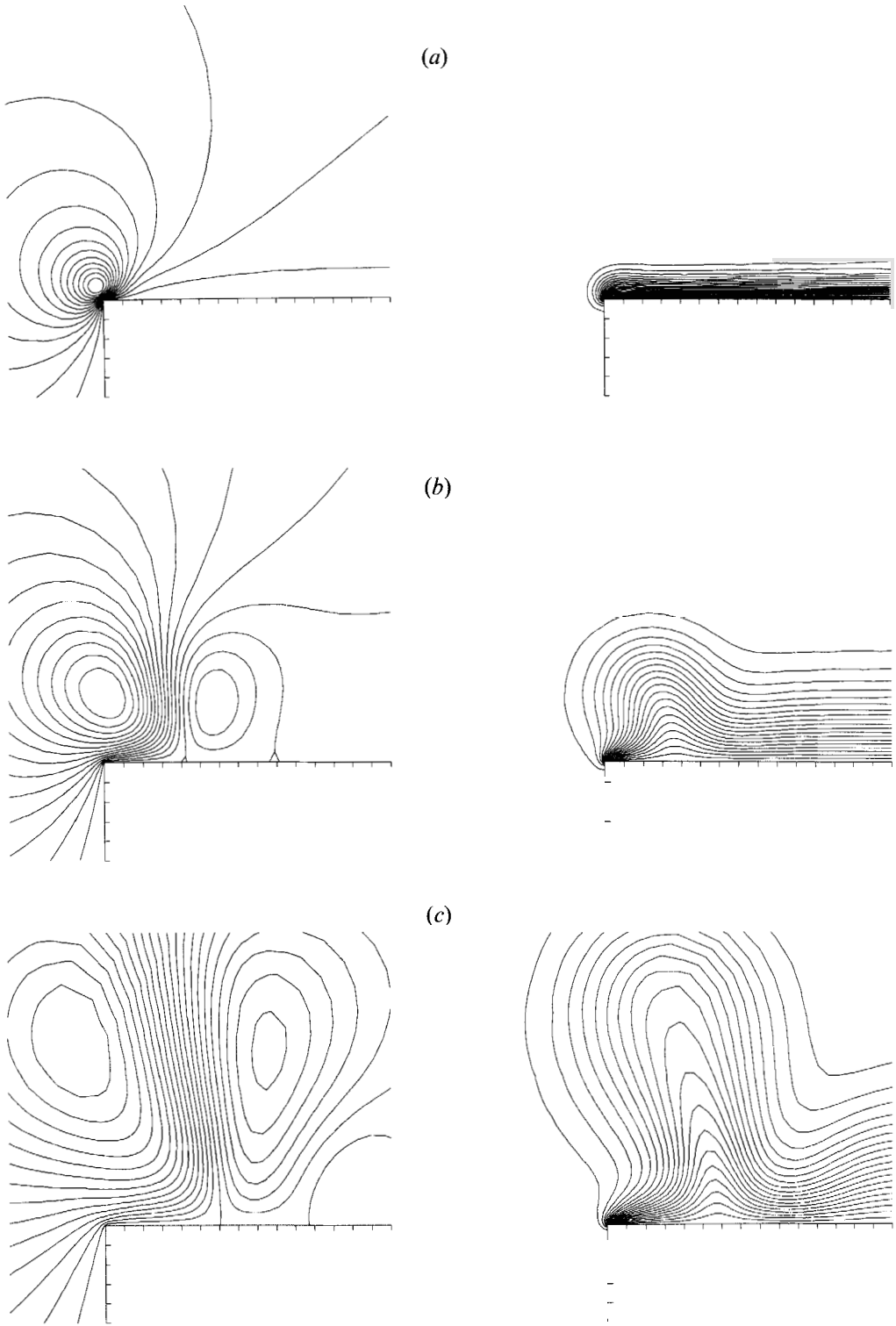


FIGURE 5. Streamlines and isotherms for the starting problem. Streamlines are on the left, the increment between streamline contours is  $\frac{1}{18}\psi_{\max}$ , and isotherms are at an interval of 0.05; these conventions also apply to figures 7 and 8. Tick marks are at intervals of 10. (a)  $t = 37$ ,  $\psi_{\max} = 1.53$ ; (b)  $t = 404$ ,  $\psi_{\max} = 6.18$ ; (c)  $t = 1046$ ,  $\psi_{\max} = 12.19$ .

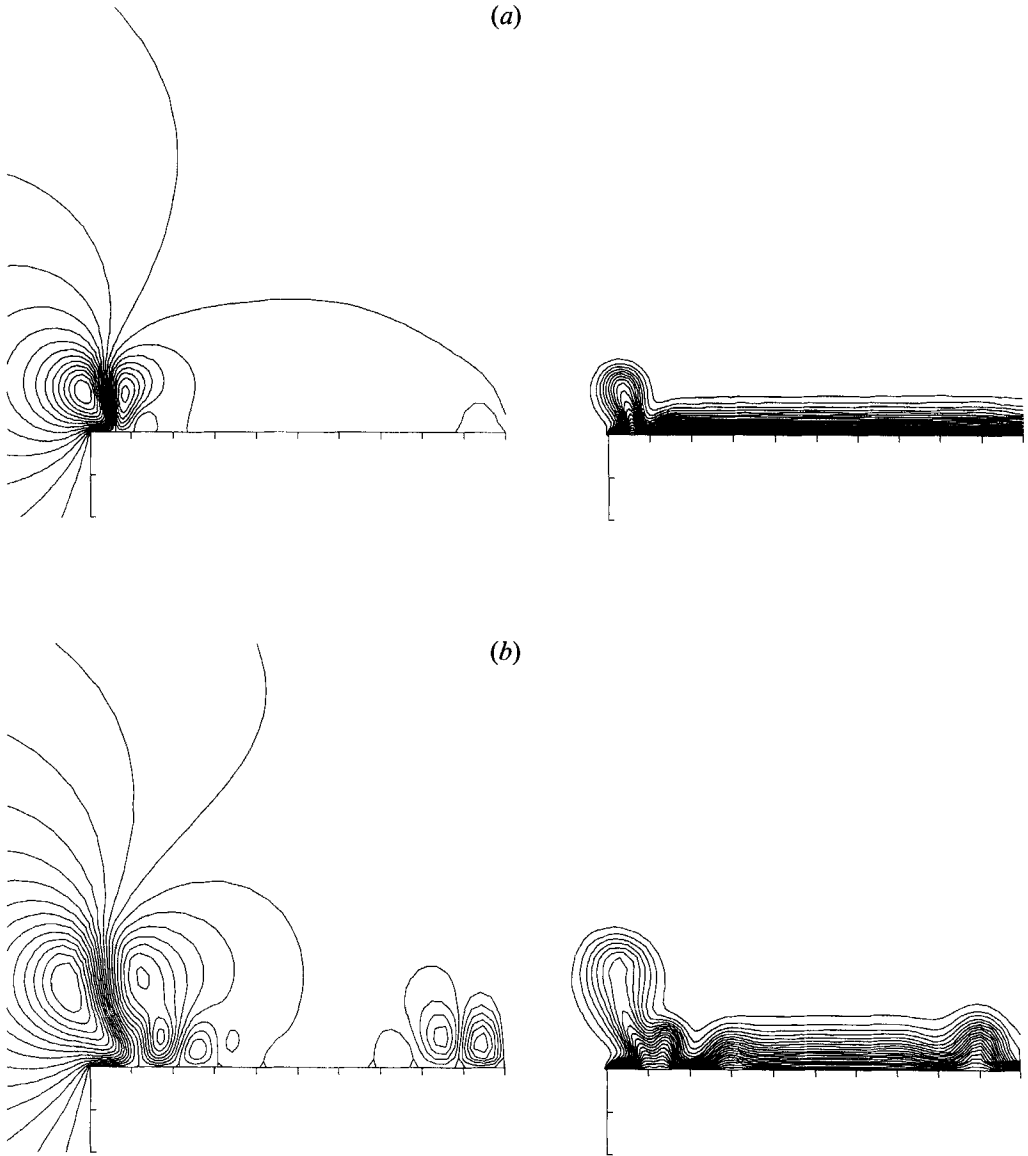


FIGURE 6(a,b). For caption see facing page.

of the plume. The plume therefore has been left as a reminder, so to speak, of the violent nature of the onset of convection, and it continues to rise buoyantly, advect with the flow induced by the boundary layer and cool gradually by diffusion. At the point in the computation represented by figure 7(b) the plume is too close to the  $\eta_{\max}$  boundary to guarantee the validity of further computation and so further numerical results have not been obtained.

## 6. The long-term dynamics

We turn now to a description and discussion of the flow and temperature field after disturbances have entered the nonlinear regime. The results we present were computed on a  $97 \times 47$  grid over 12000 time steps, and the computation ran for approximately

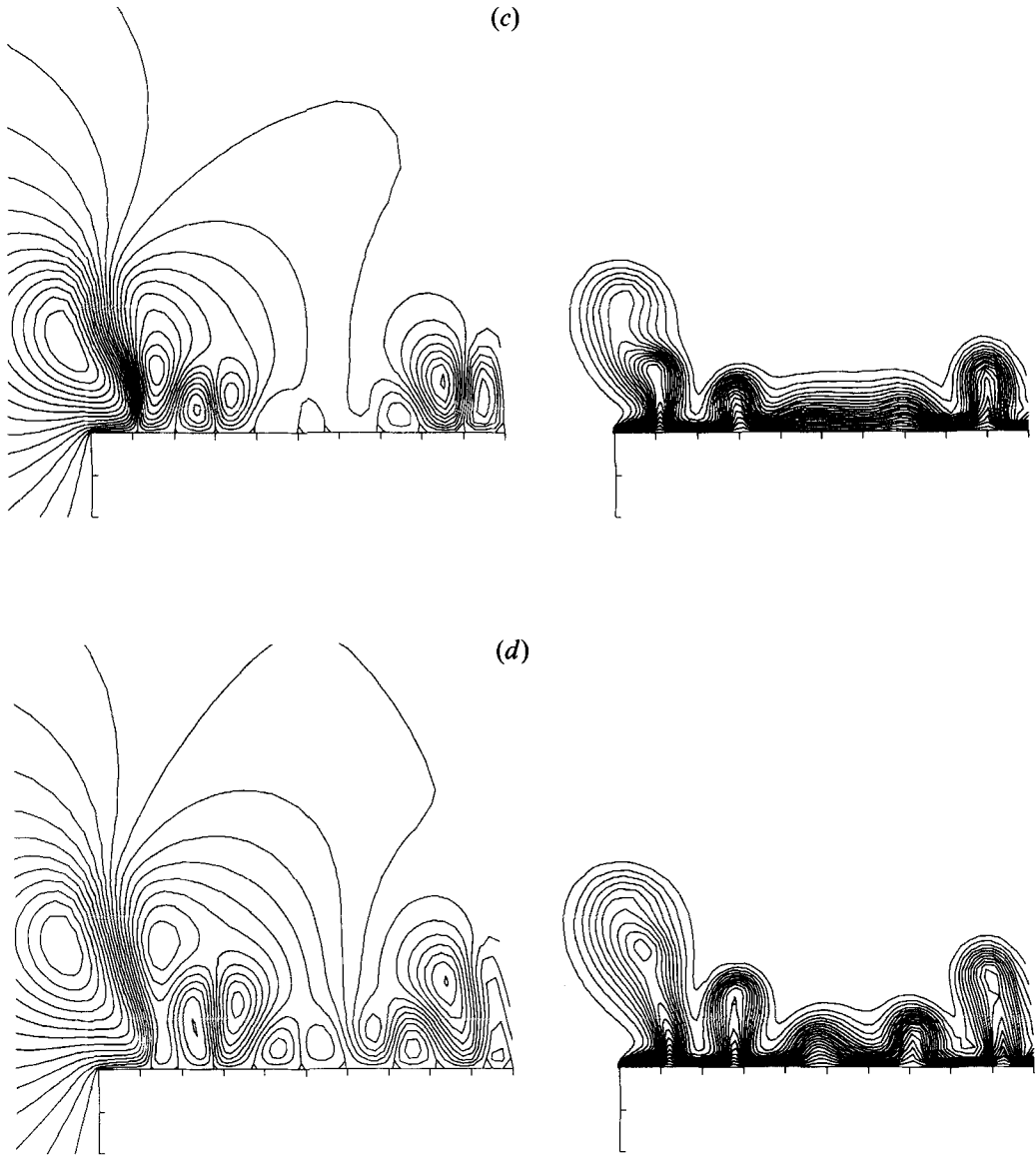


FIGURE 6. Streamlines and isotherms for the starting problem. Tick marks are at intervals of 100. (a)  $t = 1046$ ,  $\psi_{\max} = 12.19$ ; (b)  $t = 2126$ ,  $\psi_{\max} = 17.26$ ; (c)  $t = 4008$ ,  $\psi_{\max} = 37.28$ .

13 days, yielding an average time of about 1.5 minutes per time step. The grid was non-uniform in both directions, as detailed in the Appendix. The initial condition was taken to be the steady boundary-layer solution and there was, in fact, no need to introduce an artificial disturbance, as was the case in §4. This is because placing the steady boundary-layer profile (obtained as above) on the non-uniform grid proved sufficient to initiate the instability. Clearly, with such a large amount of data it is difficult to condense it sufficiently and retain all its salient features without being too detailed. Therefore we have concentrated mainly on plots of the instantaneous isotherms over the first two thirds of the computation, and have chosen not to present plots of the streamlines, although some aspects of these will be discussed.

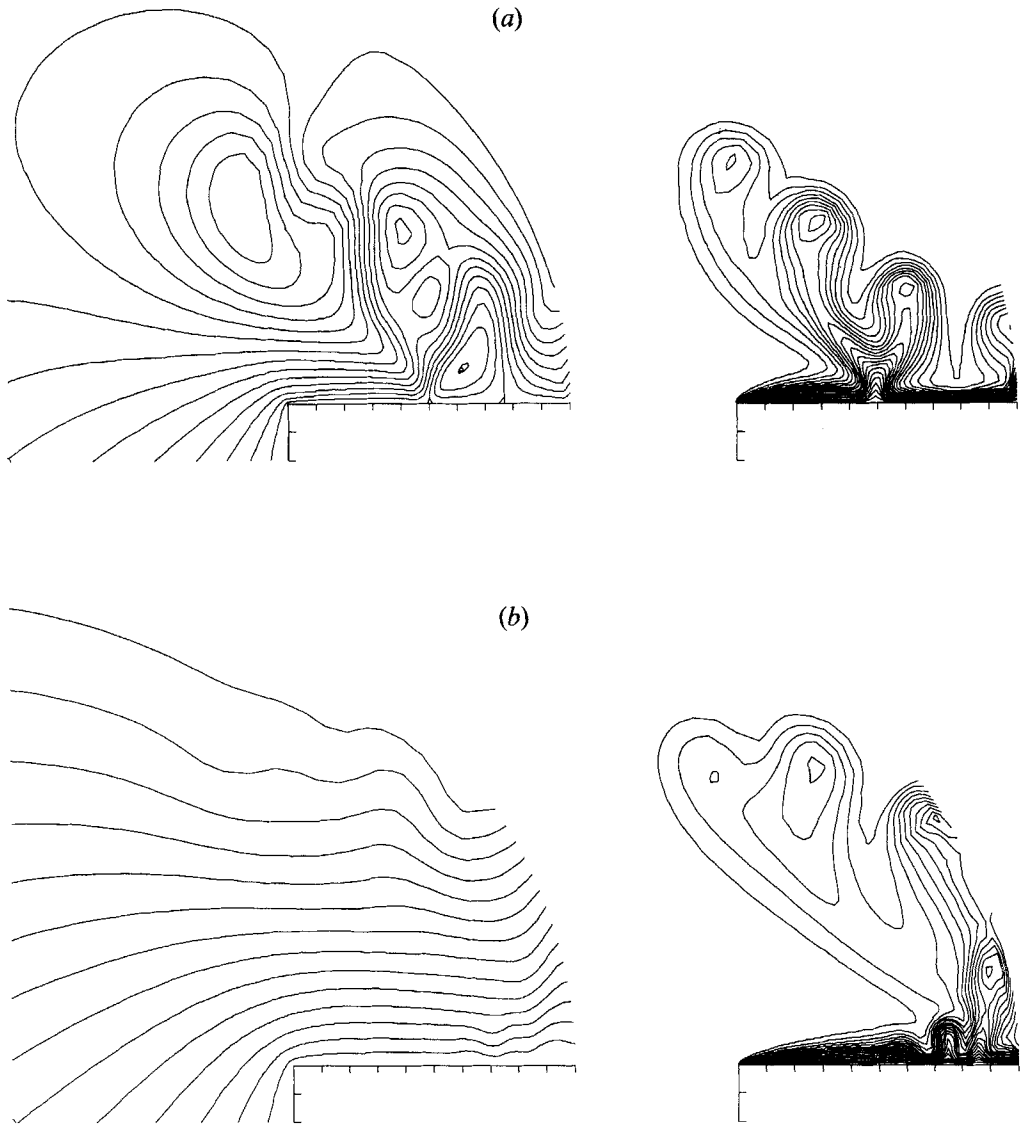


FIGURE 7. Streamlines and isotherms for the starting problem. Tick marks are at intervals of 100. (a)  $t = 7566$ ,  $\psi_{\max} = 55.13$ ; (b)  $t = 12888$ ,  $\psi_{\max} = 254.87$ .

In figure 8(*a–x*) the isotherms at different stages of evolution of the flow are shown. Instability of the basic boundary layers sets in initially as two distinct waves in the isotherms (see figure 8*a*); these we shall refer to as ‘cells’ by virtue of what the perturbation isotherm field looks like (see figure 9, which corresponds to figure 8*c*). Figure 8(*a–f*) represents the initial stages in the evolution of the disturbance. Though it is nonlinear, the disturbance is local in the sense that it has not yet propagated far downstream. As in figure 4, the development of convective motion takes place rapidly whilst advecting slowly downstream. Once in the nonlinear regime (i.e. after figure 8*a*) the cells show a marked reluctance to change their wavelength and, as they grow in strength, they soon erupt from the boundary layer to form embryonic plumes (figure 8*d*). As the pair of plumes grow a strong downward fluid motion is generated to either

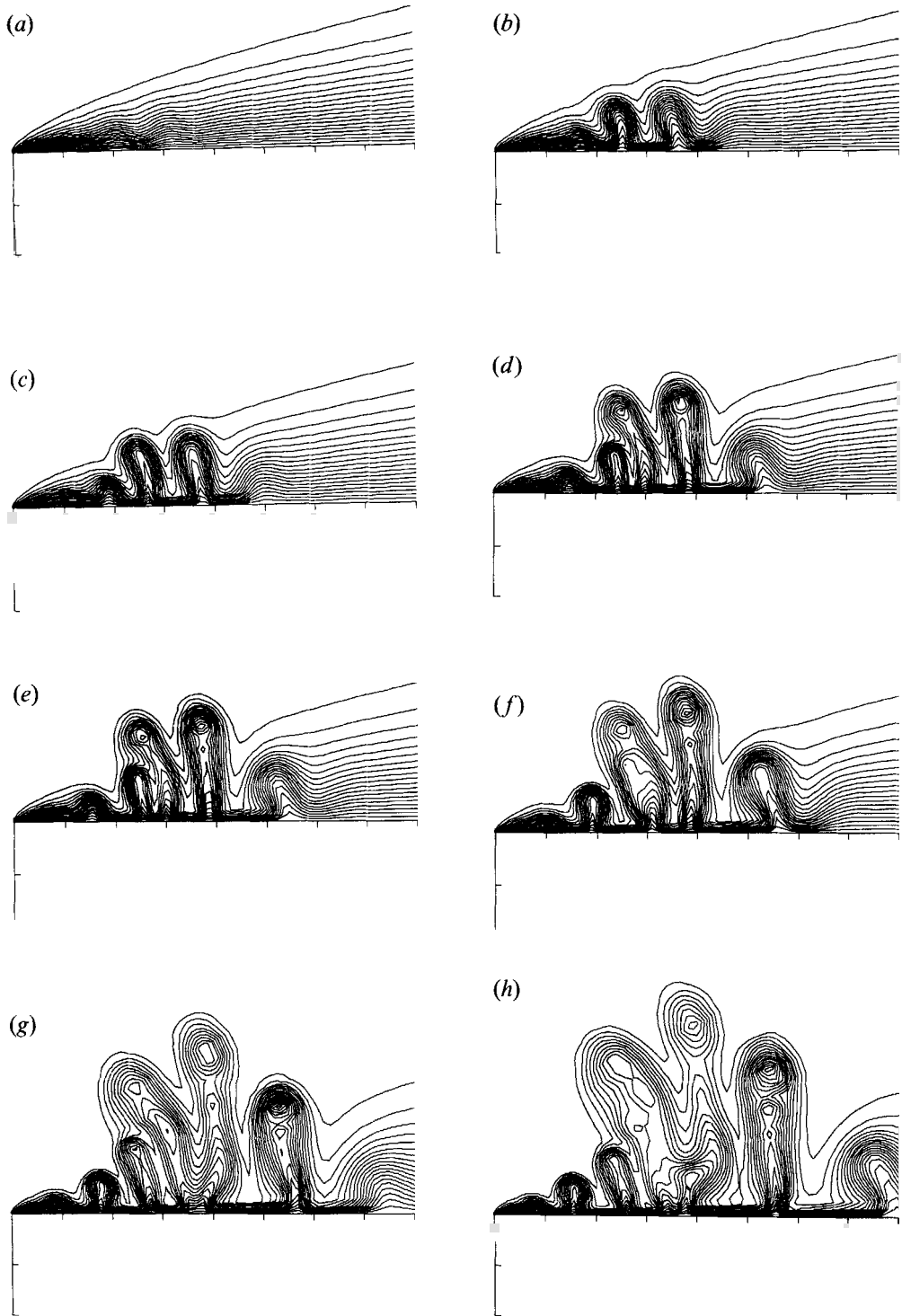


FIGURE 8(a-h). For caption see page 289.

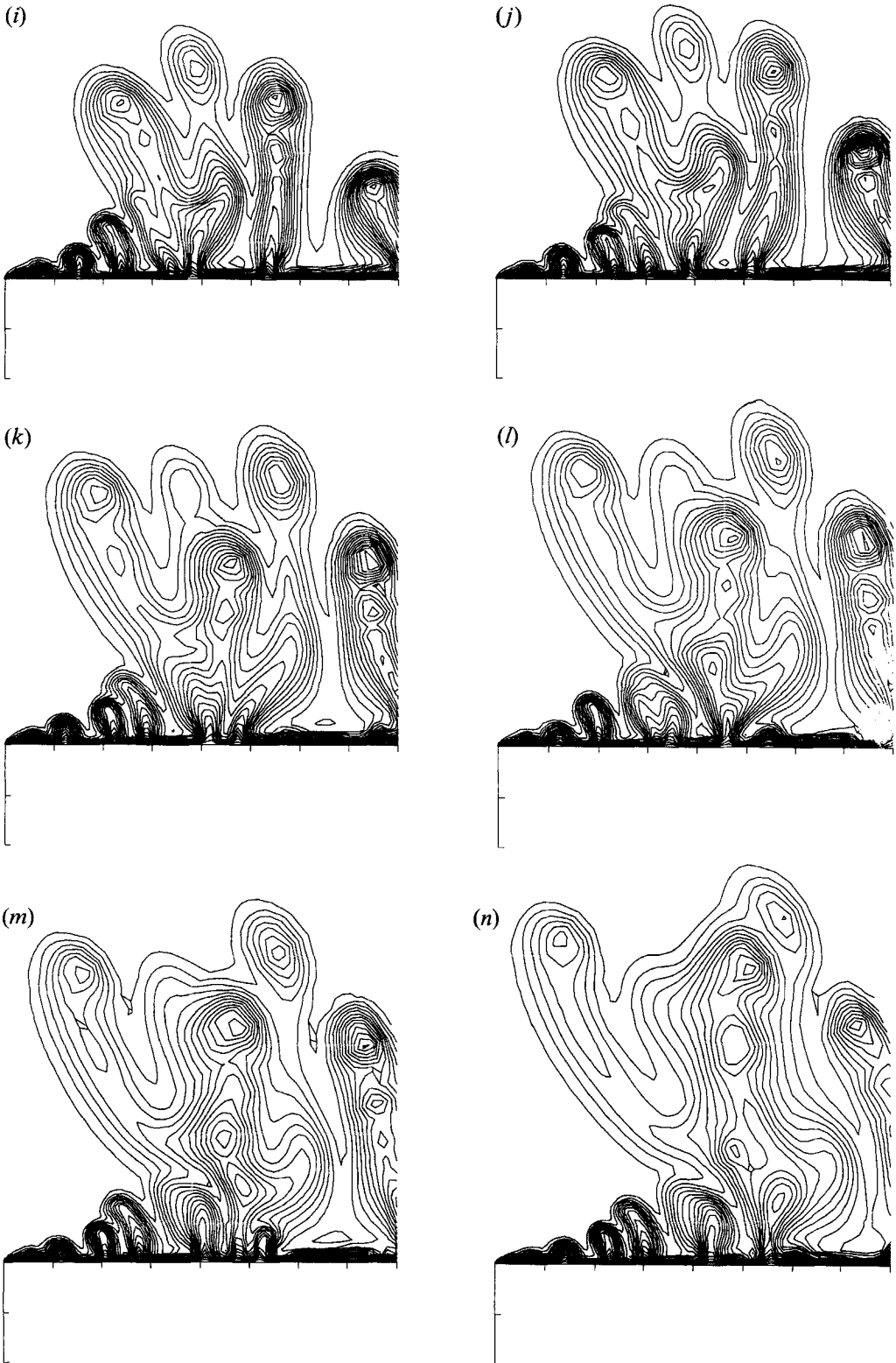


FIGURE 8(*i-n*). For caption see page 289.

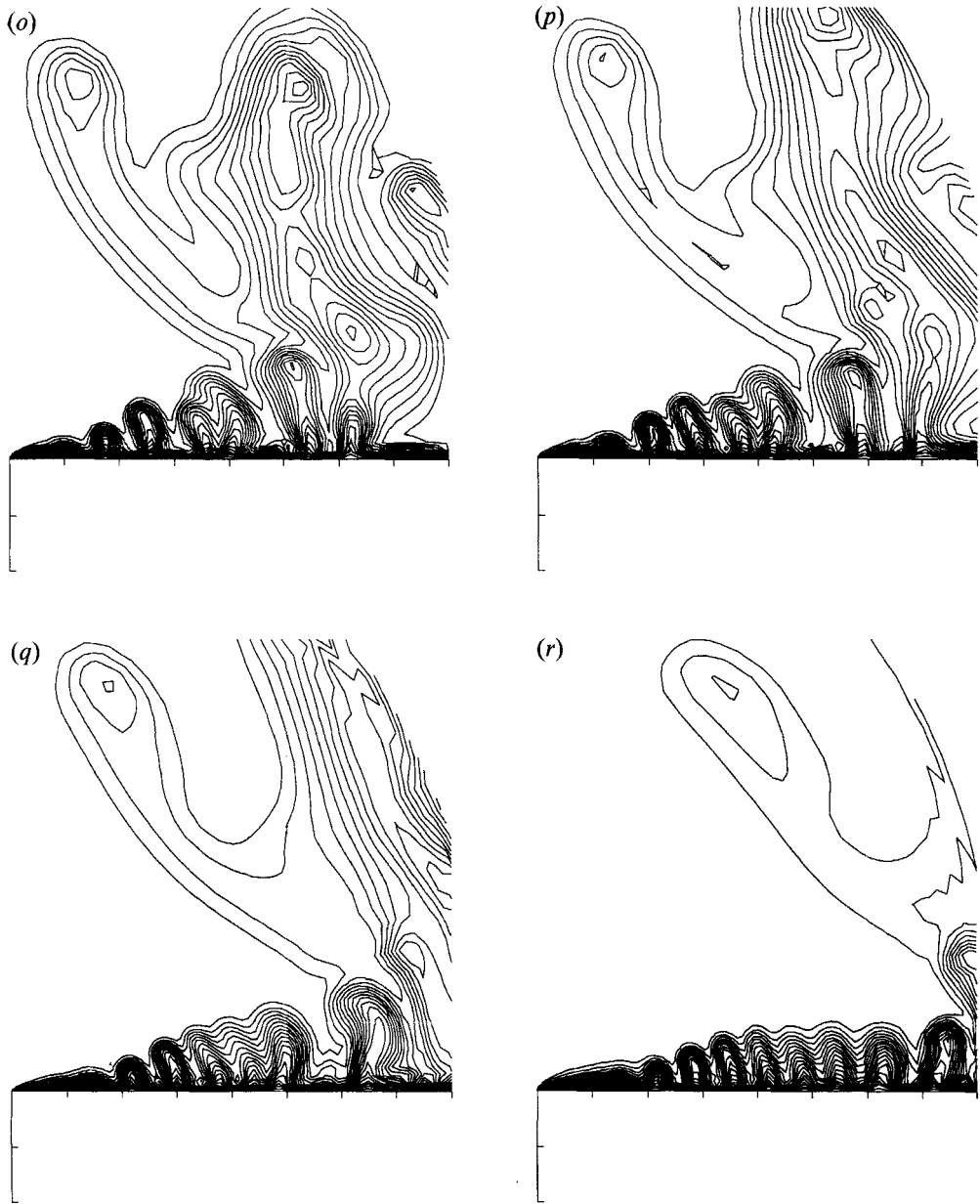


FIGURE 8(*o-r*). For caption see page 289.

side of and between the plumes, as evidenced by the concentration of isotherms near the boundary. To the left of the plumes an enhanced streamwise flow into the left-hand plume thins the boundary layer slightly near the leading edge. This is to be expected for if a steady mixed convection boundary-layer solution is sought, where there is an imposed flow of the form  $\psi = U\xi\eta$ , then it can be shown that the boundary-layer thickness decreases as  $U$  increases from 0 (note that an analogous exact solution for mixed convection induced by a vertical surface in porous media has been given in Rees & Bassom 1991). Both upstream and downstream of the plumes further cells are being generated. In fact, throughout figure 8(*c-i*) cells generated near the leading edge advect

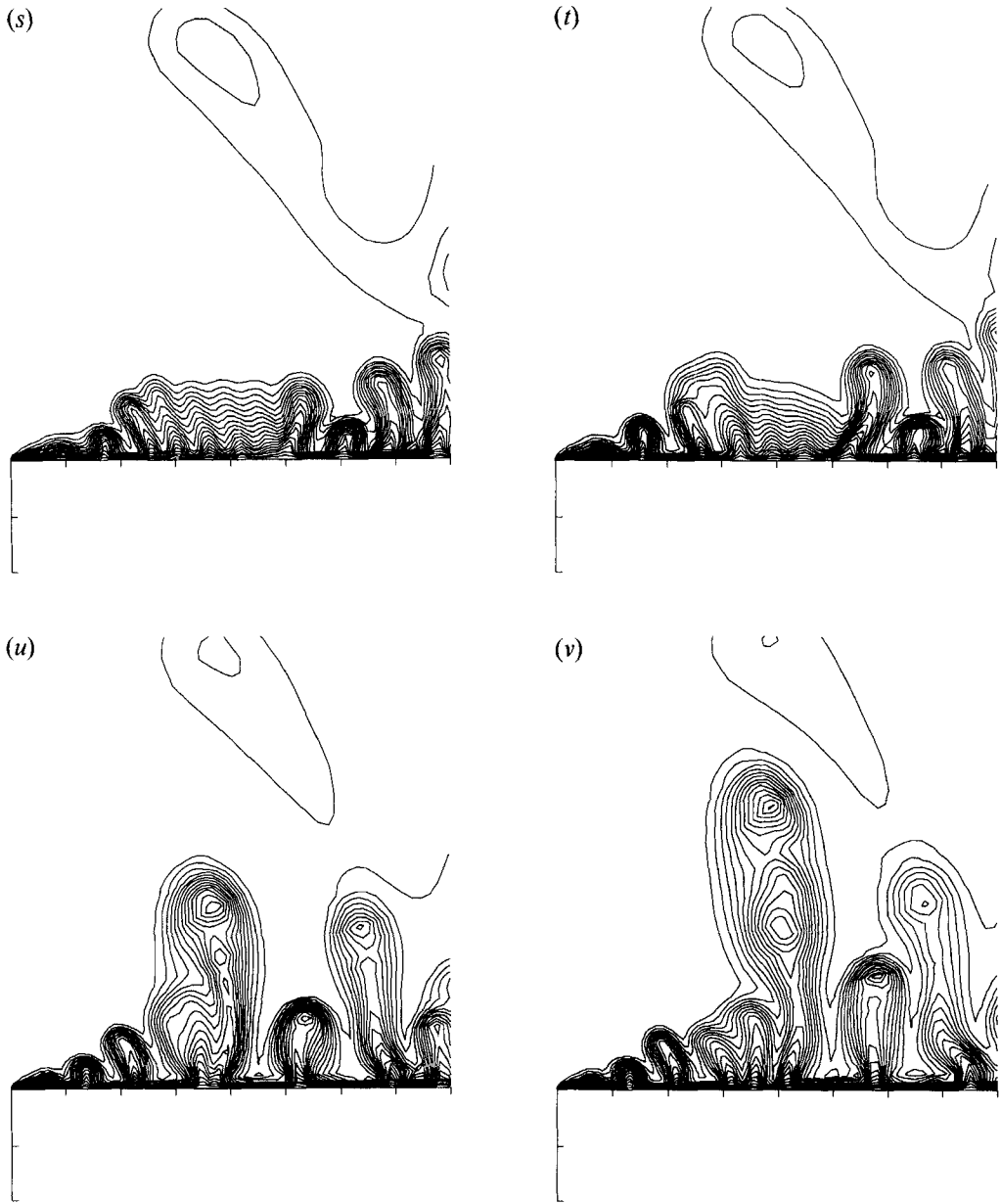


FIGURE 8(s-v). For caption see facing page.

downstream and collide with the base of the second plume. The first such collision can be seen clearly in figure 8(d); the second in figure 8(g). It is important to note that the generation of cells near the leading edge is self-propagating and takes place continuously throughout the whole computation.

By figure 8(g) a third plume has been formed downstream of the original pair and it is characterized by very strong downward fluid motion on both sides. Since a fully developed plume in isolation entrains fluid from surrounding regions it is to be expected that the plume-like features here would do the same. However, for this plume, fluid is more easily entrained from the right, and this causes the plume to be advected

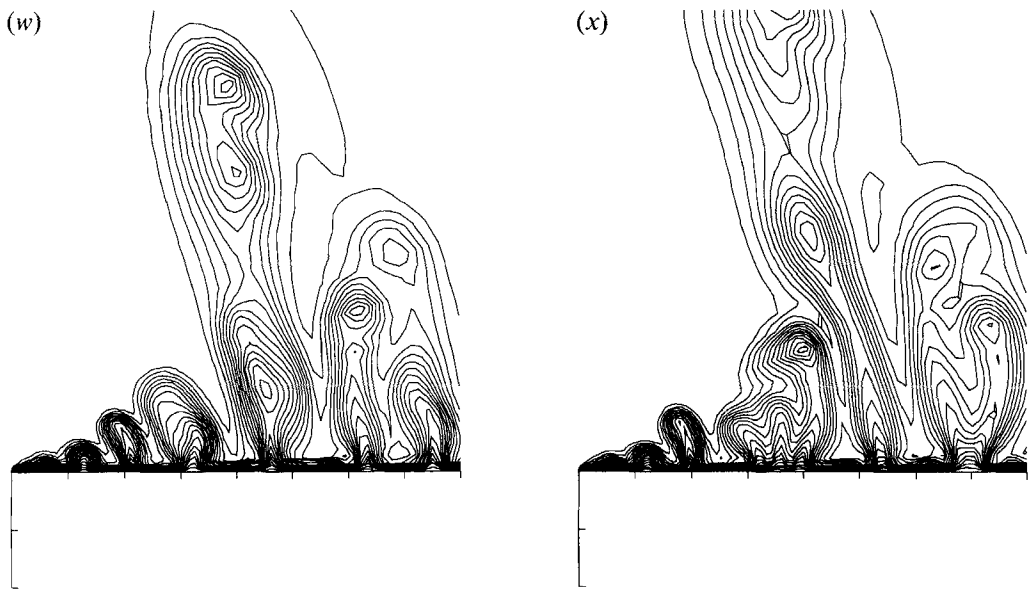


FIGURE 8. Contours of isotherms (at an interval of 0.05). (a)  $t = 3086$ ; (b)  $t = 4323$ ; (c)  $t = 4812$ ; (d)  $t = 5758$ ; (e)  $t = 5904$ ; (f)  $t = 6617$ ; (g)  $t = 7856$ ; (h)  $t = 8966$ ; (i)  $t = 10079$ ; (j)  $t = 12191$ ; (k)  $t = 13206$ ; (l)  $t = 14190$ ; (m)  $t = 15129$ ; (n)  $t = 17148$ ; (o)  $t = 18286$ ; (p)  $t = 20330$ ; (q)  $t = 22395$ ; (r)  $t = 24382$ ; (s)  $t = 27017$ ; (t)  $t = 29668$ ; (u)  $t = 31880$ ; (v)  $t = 34016$ ; (w)  $t = 36256$ ; (x)  $t = 38471$ .

leftwards towards the original pair; see the base of the plume as shown in figure 8(h–l). Such behaviour, where two plumes are drawn towards one another, is well documented in the experimental work reported by Pera & Gebhart (1975) who studied thermal plumes in fluids. We note, in passing, that the time interval between successive frames has now increased substantially from that given by figure 8(a–f). The apparent motionlessness of the cells near the leading edge is due entirely to aliasing.

The large region of warm fluid outside the original boundary layer is now slowly advecting downstream, rising buoyantly, and cooling by diffusion. Also, in figure 8(m), the ‘remains’ of cells which collided with the base of the first plume can be seen as local hot spots within the region. Once this region has cooled and risen sufficiently, the cells generated near the leading edge become decreasingly affected by it as they propagate downstream and they maintain their identity as cells rather than becoming hot spots in a plume (see figure 8(l–r)). However, as the main bulk of the warm region begins to advect out of the computational region the induced flow increases substantially in strength with the maximum value of the streamfunction over the computational domain rising quickly from near 100 to over 700. The boundary layer now thins to about half its original thickness (compare figures 8a and 8r). The resulting cellular pattern is contained within the boundary layer, has a smaller wavelength than in the beginning when the boundary layer was thicker, and cells are generated further downstream. The remaining plume, which is now much weaker, has cooled and weakened substantially, and advects quickly out of the  $\xi = \xi_{\max}$  boundary.

After the time represented by figure 8(s), the flow decreases in strength, as the plume is now far from the leading edge, and the boundary layer expands once more. There is competition between the short-wavelength cells with cell merging and extinction, and two eventually dominate, becoming plume-like, as shown in figure 8(u). The first of these rises rapidly, all the while suffering cellular collisions at its base. In figure 8(v) it can be seen to contain at least three hot spots as a result of these collisions.

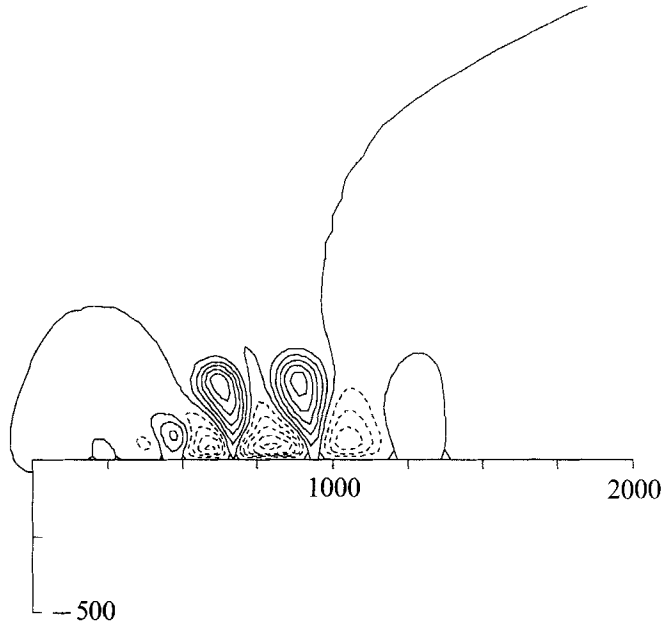


FIGURE 9. Contours for the perturbation isotherms corresponding to figure 8(c) (at an interval of 0.1, with negative isotherms dashed).

After figure 8(x), the cycle: strong plume – boundary-layer thinning – advection of the plume out of the computational domain – growth of a new dominant plume, seems to continue. Owing to computer storage requirements and the length of time taken to compute even these figures, it is difficult to be certain whether this cycle is an artifact of having the computational boundary at the value of  $\xi_{\max}$  chosen, or whether the plume was sufficiently far from the leading edge not to affect substantially the motion there. Certainly the strong motion and boundary-layer thinning takes place near the time represented by figure 8(q), which is well before the warm region leaves the computational domain. Moreover, it is possible, given a larger value of  $\xi_{\max}$ , that the boundary layer could remain relatively thin for a much longer time span. At present there is no way of deciding which factor is more important.

In figure 10(a–c) we display plots of the temperature at three different locations as a function of time. Figure 10(a), which represents a point quite close to the leading edge, clearly shows the different types of dynamical activity described above. After the short initial period during which the disturbances first grow, the generation of new cells is seen as a temporal oscillation in the temperature as they advect past the station. The period of oscillation is roughly constant, indicating that the generation mechanism is quite well behaved and independent of the formation of plumes downstream. When the flow markedly increases in strength, it has a global effect on the flow field. The thinning of the boundary layer is seen as a reduction in the temperature. Indeed this station would now seem to be upstream of where instability occurs, for the temperature profile shows no evidence of oscillations between  $t = 4500$  and  $5500$ . As the boundary-layer thickens, the temperature rises and the profile becomes oscillatory once more. From this figure it might appear that the flow should settle down and become periodic. However, the similarities between the three regions of oscillatory behaviour are deceptive since the generation of plumes, as seen in figure 9, seems to be strongly dependent on the local nonlinear interaction of cells. The means by which substantial plumes, such as those shown in figure 8(j) and 8(u), are generated are quite different

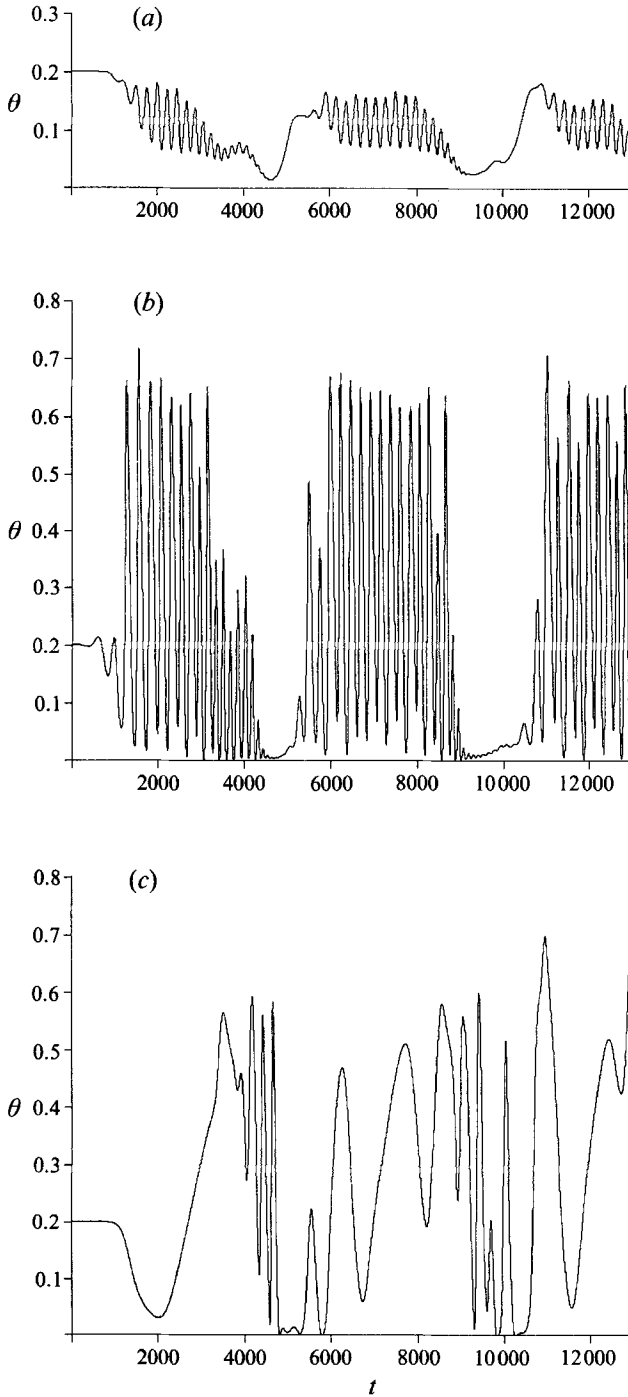


FIGURE 10. Variation in time of the temperature at chosen points in the flow field. (a)  $\xi = 16$ ,  $\eta = 2.5$ , or  $x \approx 141$ ,  $y \approx 71$ ; (b)  $\xi = 22$ ,  $\eta = 2.5$ , or  $x \approx 379$ ,  $y \approx 134$ ; (c)  $\xi = 35$ ,  $\eta = 2.5$ , or  $x \approx 1563$ ,  $y \approx 340$ .

from one another, as are the shapes of the plumes. It seems to us too unlikely, therefore, that the flow will eventually become periodic.

The evolution of temperature at a station further downstream is given in figure 10(b). Variations in temperature are greater now, but the motion of the small-wavelength cells can be seen near  $t = 9500$ . The period of the oscillation of the small-wavelength cells is relatively short. This reflects the fact that the external flow is stronger, which, in turn causes the cells to advect more quickly. Finally, in figure 10(c), we show the temperature at a point much further downstream. There is quite clearly a different timescale associated with this location, and this could well be explained by the fact that plume formation occurs upstream of the location of the point. This graph now has quite a random look to it and it could well be that the fluid motion is chaotic. Indeed, we attempted to test this idea by introducing the perturbation shown in figure 4(a)(i) to the flow represented by figure 8(h), and following its evolution until the time represented by figure 8(s). Over this period the perturbation spreads out over most of the region covered by the original boundary layer, and its maximum amplitude exhibits a slowly growing oscillation. At the end of the computation it had grown to about four times its original maximum amplitude. We would conclude that the flow is quite possibly chaotic in the sense that two initially close profiles will eventually diverge given enough time, and therefore it has a positive Lyapunov exponent. It is quite likely, therefore, that differences in procedure such as the numerical method (first or second order), different grid lengths, different time steps, different precision arithmetic, or even different coordinate transformations would eventually yield detailed results quite unlike each other. But, as mentioned earlier, consideration of computer storage requirements and computer time precludes such a survey at present.

## 7. Conclusions and discussion

In this paper we have considered various aspects of the time-dependent flow induced by a semi-infinite, horizontal, heated surface in a porous medium. This has been achieved by using a suitable coordinate transformation and an implicit time-dependent numerical scheme based on pointwise iteration accelerated by the Full Approximation Scheme multigrid technique. Considerations of the linear and nonlinear stability of the basic flow were facilitated by the existence and use of an exact solution. Certain difficulties associated with the choice of a finite computational domain, including the problems of selecting the appropriate boundary conditions and the implications of such a selection have been discussed earlier.

Our main result, from the point of view of boundary-layer stability theory, is described in detail in §6, and is concerned with the nonlinear evolution of wave disturbances. Small disturbances grow rapidly in strength and quickly enter the nonlinear regime whilst moving only a small distance downstream relative to their wavelength. It seems that these nonlinear waves tend to maintain their wavelength as they develop and travel downstream. However the process of cell merging is a means by which their wavelength can remain roughly comparable with the local boundary-layer thickness. Sometimes cellular merging precipitates the generation of a plume which then distrupts the external flow field substantially. The resulting increased entrainment into the boundary layer on the leading-edge side of the plume thins the boundary layer locally and temporarily inhibits or delays instability.

All the dynamical phenomena described above are attributable to both the presence of nonlinear terms in the governing equations and the retention of streamwise derivatives in the diffusion and advection terms. Traditional theory using the parallel-

flow approximation neglects all streamwise derivatives and is, in general, a linear theory (but note that a recent exception is the weakly nonlinear work of Chen *et al.* 1991). The more recently developed, and more powerful non-parallel methods are usually restricted to regimes where the boundary-layer approximation is valid, and to wavelengths which are scaled on the boundary-layer thickness. Thus they are valid at asymptotically large distances downstream of the leading edge. This type of theory also neglects streamwise derivatives in the diffusion terms and thus the disturbance equations are parabolic partial differential equations. This forms the basis for Hall's Görtler vortex analyses and other receptivity studies, for a disturbance is introduced at a fixed point in the boundary layer for all time and its evolution downstream is followed. This neglect of the streamwise diffusion terms, though justified in a formal asymptotic sense, cannot allow disturbances to be self-propagating, as presented here.

For the present problem there is a somewhat quick spatial transition between regimes where (i) disturbances decay (i.e. close to the leading edge), (ii) disturbances grow to form what is a roughly regular train of travelling waves, as illustrated by figure 10(a), and (iii) distinctly aperiodic or perhaps chaotic motion exists. This, we believe, is rather atypical of boundary-layer flows in general. The point beyond which disturbances grow is usually at a location where the basic boundary-layer flow is much more accurate than that presented here. The onset of secondary instability, which begins the route to turbulence, then takes place a large number of cellular wavelength further downstream (see, for example, the schematic of the transition between convective regimes for the vertical free convection problem discussed by Gebhart (1979; figure 13). For more typical boundary layers then, we expect that the flow near the leading edge will not be greatly affected by instabilities occurring far downstream. Therefore it should not prove necessary to include the leading edge in the computational domain – this would allow the use of much faster explicit or pseudo-implicit methods (such as DuFort–Fraenkel). The use of an orthogonal grid reflecting the shape of the boundary layer should nevertheless be retained, for reasons of economy of computer storage space. For convective boundary layers the local Rayleigh or Grashof number does not grow so rapidly downstream, and therefore the onset of aperiodicity will not be so precipitate. Unfortunately, such analyses will require the use of an accurate numerical representation of the basic flow.

Finally it is necessary to comment briefly on the three-dimensional aspects of the present flow. We have already discussed the qualitative contradiction between the experimental evidence cited in Hsu *et al.* and the results of linear theories based on the parallel-flow approximation. There is therefore a clear need to extend our computational work to three dimensions to investigate whether vortices or waves are the dominant primary mode of instability. In the analogous problem of thermal convection of a fluid induced by a heated horizontal surface the primary mode of instability is the spanwise-periodic vortex, but this pattern breaks down into a time-dependent motion before becoming fully turbulent. In this fluid problem the width of the boundary layer increases fairly slowly with the distance downstream and hence the (fixed) wavelength of a vortex decreases slowly compared with the local boundary-layer width. This allows the nonlinear vortex to become well-established before it is destabilized by oblique Tollmien–Schlichting waves further downstream. For the present problem the boundary layer width varies quickly and hence the wavelength of a vortex will decrease quickly compared with the local boundary-layer width. We think that it is possible that a nonlinear vortex structure could very well be *unstable* to oblique wave disturbances over the whole domain. Such a possibility could be reconciled with the cited experimental results of Hsu *et al.* by appealing to the effects

of geometrical boundaries in restricting an oblique mode mechanism. We fully intend to pursue time-dependent three-dimensional computations in order to clarify the above speculations and to attempt to reconcile the results of approximate methods with experimental results. The tasks facing us are the following: the determination of a steady nonlinear vortex structure; the determination of allowable wavelengths of vortex; the possibility of oblique vortex structures; the instability of vortices to two-dimensional or oblique wave disturbances; the instability of two-dimensional flow to three-dimensional disturbances; and the investigation of the transition to turbulence. The accomplishment of the first of these tasks will determine which mode, a vortex or a wave, appears nearer the leading edge. This will represent the first precise study of the relative importance of waves and vortices in a growing thermal boundary layer. We intend to report on these developments in the future.

The authors would like to thank the referees for their useful comments.

### Appendix. The coordinate-stretching transformations

We present here details of the coordinate stretching transformation used to increase the efficiency of the numerical method. A stretched  $\xi$ -coordinate,  $\bar{\xi}$ , is defined according to the formulae:

$$\begin{aligned}\xi &= 4\bar{\xi}, & 0 \leq \bar{\xi} \leq 4, \\ \xi &= 16 + 4(\bar{\xi} - 4) - \frac{8}{9}(\bar{\xi} - 4)^3 + \frac{1}{3}(\bar{\xi} - 4)^4 - \frac{1}{27}(\bar{\xi} - 4)^5, & 4 \leq \bar{\xi} \leq 7, \\ \xi &= (\bar{\xi} - 7) + 22, & 7 \leq \bar{\xi};\end{aligned}$$

whilst a stretched  $\eta$ -coordinate,  $\bar{\eta}$ , is given by the formulae:

$$\begin{aligned}\eta &= \bar{\eta}, & 0 \leq \bar{\eta} \leq 3, \\ \eta &= \bar{\eta} + \frac{2}{9}(\bar{\eta} - 3)^3 - \frac{1}{27}(\bar{\eta} - 3)^4, & 3 \leq \bar{\eta} \leq 6, \\ \eta &= 3(\bar{\eta} - 6) + 9, & 6 \leq \bar{\eta}.\end{aligned}$$

These transformations were designed so that not only are  $\xi$  and  $\eta$  continuous functions of  $\bar{\xi}$  and  $\bar{\eta}$ , respectively, but so are their first and second derivatives.

### REFERENCES

- ARAKAWA, A. 1966 Computational design of long-term numerical integration of the equations of fluid motion: I. Two-dimensional incompressible flow. *J. Comput. Phys.* **1**, 119–143.
- BASSOM, A. P. & REES, D. A. S. 1993 The linear vortex development of boundary layer flow induced by an inclined heated surface in a porous medium. Department of Mathematics, University of Exeter, Preprint M18-92. Submitted to *Q. J. Mech. Appl. Maths.*
- BRANDT, A. 1984 *Multigrid Techniques: 1984 Guide with Applications to Fluid Dynamics*. Lecture Notes in C.F.D. at the Von Karman Institute for Fluid Dynamics; *GMD-Studien*, vol. 85. Bonn: GmD mbH.
- CHANG, I. D. & CHENG, P. 1983 Matched asymptotic expansions for free convection about an impermeable horizontal surface in a porous medium. *Intl J. Heat Mass Transfer* **26**, 163–174.
- CHEN, C. C., LABHABI, A., CHANG, H.-C. & KELLY, R. E. 1991 Spanwise pairing of finite-amplitude longitudinal vortex rolls in inclined free-convection boundary layers. *J. Fluid Mech.* **231**, 73–111.
- CHENG, P. 1978 Heat transfer in geothermal systems. *Adv. Heat Transfer* **14**, 1–105.
- CHENG, P. & CHANG, I. D. 1976 Buoyancy induced flows in a porous medium adjacent to impermeable horizontal boundaries. *Intl J. Heat Mass Transfer* **19**, 1267–1272.
- CHENG, P., HSU, C. T. 1984 Higher order approximations for Darcian free convection about a semi-infinite vertical flat plate. *Trans. ASME C: J. Heat Transfer* **106**, 143–151.

- CHENG, P. & MINKOWYCZ, W. J. 1977 Free convection about a vertical flat plate imbedded in a porous medium with application to heat transfer from a dike. *J. Geophys. Res.* **82**, 2040–2044.
- DANIELS, P. G. & SIMPKINS, P. G. 1984 The flow induced by a heated vertical wall in a porous medium. *Q. J. Mech. Appl. Maths* **37**, 339–354.
- EAGLES, P. M. 1980 A Bénard convection problem with a perturbed lower wall. *Proc. R. Soc. Lond. A* **371**, 359–379.
- GEBHART, B. 1979 Buoyancy induced fluid motions characteristic of applications in technology. (The 1978 Freeman Scholar Lecture.) *Trans. ASME I: J. Fluids Engng* **101**, 5–28.
- HALL, P. 1982a Taylor–Görtler vortices in fully developed or boundary-layer flows: linear theory. *J. Fluid Mech.* **124**, 475–494.
- HALL, P. 1982b On the nonlinear evolution of Görtler vortices in non-parallel boundary layer flows. *J. Inst. Maths Applics.* **29**, 173–196.
- HALL, P. 1983 The linear development of Görtler vortices in growing boundary layers. *J. Fluid Mech.* **130**, 41–58.
- HALL, P. 1990 Görtler vortices in growing boundary layers: the leading edge receptivity problem, linear growth and the nonlinear breakdown stage. *Mathematika* **37**, 151–189.
- HSU, C. T. & CHENG, P. 1979 Vortex instability in buoyancy induced flow over inclined heated surfaces in porous media. *Trans. ASME C: J. Heat Transfer* **101**, 660–665.
- HSU, C. T., CHENG, P. & HOMSY, G. M. 1978 Instability of free convection flow over a horizontal impermeable surface in a porous medium. *Intl J. Heat Mass Transfer* **21**, 1221–1228.
- IYER, P. A. & KELLY, R. E. 1974 The stability of laminar free convection flow induced by a heated inclined plate. *Intl J. Heat Mass Transfer* **17**, 517–525.
- JANG, J. Y. & CHANG, W. J. 1989 Maximum density effects on vortex instability of horizontal and inclined buoyancy induced flows in porous media. *Trans. ASME C: J. Heat Transfer* **111**, 572–574.
- KELLER, H. B. & CEBECI, T. 1971 Accurate numerical methods for boundary layer flows. I. Two-dimensional laminar flows. *Proc. Intl Conf. Num. Meth. in Fluid Dyn.* Lecture Notes in Physics, vol. 8. Springer.
- KLEISER, L. & ZANG, T. A. 1991 Numerical simulation of transition in wall-bounded shear flows. *Ann. Rev. Fluid Mech.* **23**, 495–537.
- LAPWOOD, E. R. 1948 Convection of a fluid in a porous medium. *Proc. Camb. Phil. Soc.* **44**, 508–521.
- PERA, L. & GEBHART, B. 1975 Laminar plume interactions. *J. Fluid Mech.* **68**, 259–271.
- PRATS, M. 1967 The effect of horizontal fluid on thermally induced convection currents in porous mediums. *J. Geophys. Res.* **71**, 4835–4838.
- REES, D. A. S. & BASSOM, A. P. 1991 Some exact solutions for free convective flows over heated semi-infinite surfaces in porous media. *Intl J. Heat Mass Transfer* **34**, 1564–1567.
- REES, D. A. S. & BASSOM, A. P. 1992 The linear wave instability of boundary layer flow induced by a heated horizontal surface in porous media. *University of Bath, School of Mech. Engng Rep.* 087/1992. Submitted to *Intl Com. Heat Mass Transfer*.
- REES, D. A. S. & RILEY, D. S. 1986 Free convection in an undulating saturated porous layer: resonant wavelength excitation. *J. Fluid Mech.* **166**, 503–530.
- RILEY, D. S. & REES, D. A. S. 1985 Non-Darcy natural convection from arbitrarily inclined heated surfaces in saturated porous media. *Q. J. Mech. Appl. Maths* **38**, 277–295.
- RILEY, D. S. & WINTERS, K. H. 1991 Time-periodic convection in porous media: the evolution of Hopf bifurcations with aspect ratio. *J. Fluid Mech.* **223**, 457–474.
- SMITH, F. T. 1979 On the non-parallel flow stability of the Blasius boundary layer. *Proc. R. Soc. Lond. A* **366**, 91–109.
- TIEN, C. L. & VAFAI, K. 1989 Convective and radiative heat transfer in porous media. *Adv. Appl. Mech.* **27**, 225–281.
- WALTON, I. C. 1982 On the onset of Rayleigh–Bénard convection in a fluid layer of slowly increasing depth. *Stud. Appl. Maths* **67**, 199–216.
- WALTON, I. C. 1985 The effect of a shear flow on convection in a layer heated non-uniformly from below. *J. Fluid Mech.* **154**, 303–319.